Modeling the energy trade-off between glycogen and polyphosphate use in phosphate accumulating organisms

Maria Beatriz Diniz

5158931

In partial fulfillment of the requirements for the degree of

Master of Science in Life Science & Technology

At the Delft University of Technology,

to be defended publicly on Thursday, November 11, 2021, at 13:30.

Project duration: Jan 2021 – Nov 2021

Supervision:

Ir. T. Páez Watson	TU Delft
Dr. S.A. Wahl	TU Delft

Thesis committee:

Prof.dr.ir. M.C.M van Loosdrecht	TU Delft
Dr. S.A. Wahl	TU Delft
Dr. R. González Cabaleiro	TU Delft

TU Delft

Firstly, I would like to thank Professor Aljoscha for giving me the opportunity to work on this project under his supervision. Additionally, I would like to thank all the EBT members for welcoming me into their group and helping me along the way.

I would also like to thank my family and friends for all their support. Especially, my grandfather for those car ride conversations that got me interested in science.

Lastly, but just as importantly, I would like to thank Timmy for all its unceasing help and supervision.

Phosphate accumulating organisms (PAOs) perform a storage polymer metabolism within an anaerobic-aerobic cycle. Anaerobically, PAOs take up volatile fatty acids (VFA) and store them as poly-ß-hydroxyalkanoates (PHA). The energy (mainly ATP) necessary for the transport and storage of VFA (and general maintenance) is obtained through the cleavage of polyphosphate. While the reducing equivalents (e.g. NADH) for VFA storage are obtained through the cleavage of glycogen and/or from the anaerobic operation of the TCA cycle. Aerobically, PAOs replenish their reserves of polyphosphate and glycogen, resulting in P uptake, whilst degrading PHA to obtain a carbon and energy supply for growth.

PAOs have the metabolic flexibility to adapt the synthesis of each polymer according to the resources available in the environment, and thus affecting the growth of the organism. Hence, within a PAOs metabolism, there is a trade-off between the use of glycogen and polyphosphate. This trade-off is dependent on the cell's requirements to obtain ATP and NADH for PHA storage. In turn, ATP and NADH amounts can be obtained in different ratios depending on the active metabolic routes. This thesis aims to determine what is the mechanism controlling this trade-off and if there are limits to this relationship.

To investigate this trade-off, a metabolic model for PAOs was created and simulated through a conditional flux balance analysis (cFBA) approach. The resulting amounts of the metabolites simulated with this approach were comparable to those obtained experimentally (figure 6). Additionally, this model was simulated to different sets of starting amounts of glycogen and polyphosphate at a constant acetate feed of 3.84 $mCmol/g_{dw}$, and the resulting growth was compared between each simulation. This led to an optimal range of initial polyphosphate amounts [2.1-23.5 $mPmol/g_{dw}$] and initial glycogen amounts [0.3-1 $mCmol/g_{dw}$]. In reality, these glycogen amounts were never observed experimentally and to the extent of our knowledge never have been reported in PAOs literature. This suggests a glycogen minimal limit amount (e.g. 1 $mCmol/g_{dw}$), that might reveal a robustness mechanism employed by PAOs to guarantee survivability in uncertain environments. In parallel, a thermodynamic analysis was performed on the malate dehydrogenase reaction, which led to the conclusion that this reaction is not feasible in an anaerobic environment, potentially highlighting a control mechanism.

TABLE OF CONTENTS

1

INTRODUCTION

Wastewater treatment is an essential sanitary service to society, that aims to remove contaminants from wastewater. This is done by a combination of biological, biochemical, chemical, and mechanical processes (van Loosdrecht et al., 2016).

The biological process for the removal of contaminants is achieved through the interactions and growth of microbial communities. Wastewater treatment takes advantage of communities with specific metabolic capacities that lead to the removal of certain contaminants. These metabolic traits often use storage polymers. Polymers act as carbon and energy reserves, that can be used for growth when the external substrate is depleted.

Storage polymers are particularly important in an Enhanced Biological Phosphorous Removal (EBPR) system, which relies on phosphate accumulating organisms (PAOs) and their polymer metabolism (Vargas et al., 2013). PAOs are able to take up phosphate and store it intercellularly as polyphosphate, take up carbon sources, such as Volatile fatty acids (VFAs), and store them intercellularly as poly-ß-hydroxyalkanoates (PHA), and are also able to use Glycogen as a reducing power source (Oehmen et al., 2007).

As one might expect, the waste to be treated is not constant and experiences load fluctuations, especially in domestic wastewater treatment. These fluctuations can lead to unpredictable periods of substrate scarcity, which can affect the metabolism and growth of the bacteria present, especially on the intracellular levels of storage polymers (van Loosdrecht et al., 2016). To survive these everchanging environmental conditions, PAOs possess certain metabolic flexibility when it comes to polymers, where there is a trade-off between the resources available in the environment, growth, and the synthesis of each polymer.

In this work, we explored the energy trade-off in PAOs polymer metabolism. Namely, we analyzed the trade-off between polyphosphate and glycogen and its effect on growth. This was done through system biology modeling, more specifically using a conditional flux balance analysis (cFBA), with a combination of experimental work. The following subchapters will provide further information about PAOs, EBPR, cFBA, and the energy trade-off.

1.1-PHOSPHATE ACCUMULATING ORGANISMS (PAOS) IN WASTEWATER TREATMENT

Eutrophication is caused by the growth of photosynthetic organisms, such as algae, and is stimulated by the presence of Phosphorus (P) in water bodies. Hence, there is a need to control and remove P from wastewater, in a way to avoid adverse effects on aquatic communities (Oehmen et al., 2007). Enhance Biological Phosphate removal (EBPR) is a process widely applied to P removal and is achieved by cycling activated sludge through anaerobic and aerobic phases, where carbon is only available anaerobically, creating simultaneous feast-famine cycles (Figure 1). Alternating these two phases (anaerobic- feast; aerobic-famine) enriches for Phosphate accumulating organisms (PAOs) (Majed et al., 2012).

Phosphate accumulating organisms (PAOs) are heterotrophic organisms with the distinctive capability of storing and using polyphosphate as a way to produce energy (ATP), leading to P removal from the bulk liquid phase via PAO cell removal in the waste activated sludge (van Loosdrecht et al., 2016). Anaerobically, PAOs take up volatile fatty acids (VFA), such as acetate (Ac) and propionate (Pr), and store them intercellularly as poly-ß-hydroxyalkanoates (PHA). The energy necessary for the transport and storage of VFA (and general maintenance) is obtained with the cleavage of polyphosphate (PolyP), while the reducing equivalents for these reactions are obtained with the cleavage of internally stored glycogen and/or from the anaerobic operation of the TCA cycle (Oyserman et al., 2016). Aerobically, PAOs replenish their reserves of polyphosphate and glycogen, resulting in P uptake, whilst degrading PHA to obtain a carbon and energy supply for growth (Figure 1). The metabolism carried out by PAOs is also referred to as polyphosphate accumulating metabolism (PAM). Additionally, PHA in the PAO phenotype is mainly composed of poly-β-hydroxybutyrate (PHB), poly-β-hydroxyvalerate (PHV), and poly-β-hydroxy-2-methylvalerate (PH2MV) (Oehmen et al., 2007). Their relative weight and stored amounts depend on the VFA composition (Ac or Pr). For an enriched PAO culture where acetate is the main carbon source, PAOs store mostly VFA as PHB (up to 90%) (Smolders et al., 1994). In contrast, when propionate is the main carbon source PAOs store VFA as PHV and PH2MV up to 45% of the total PHA stored (Oehmen et al., 2007).

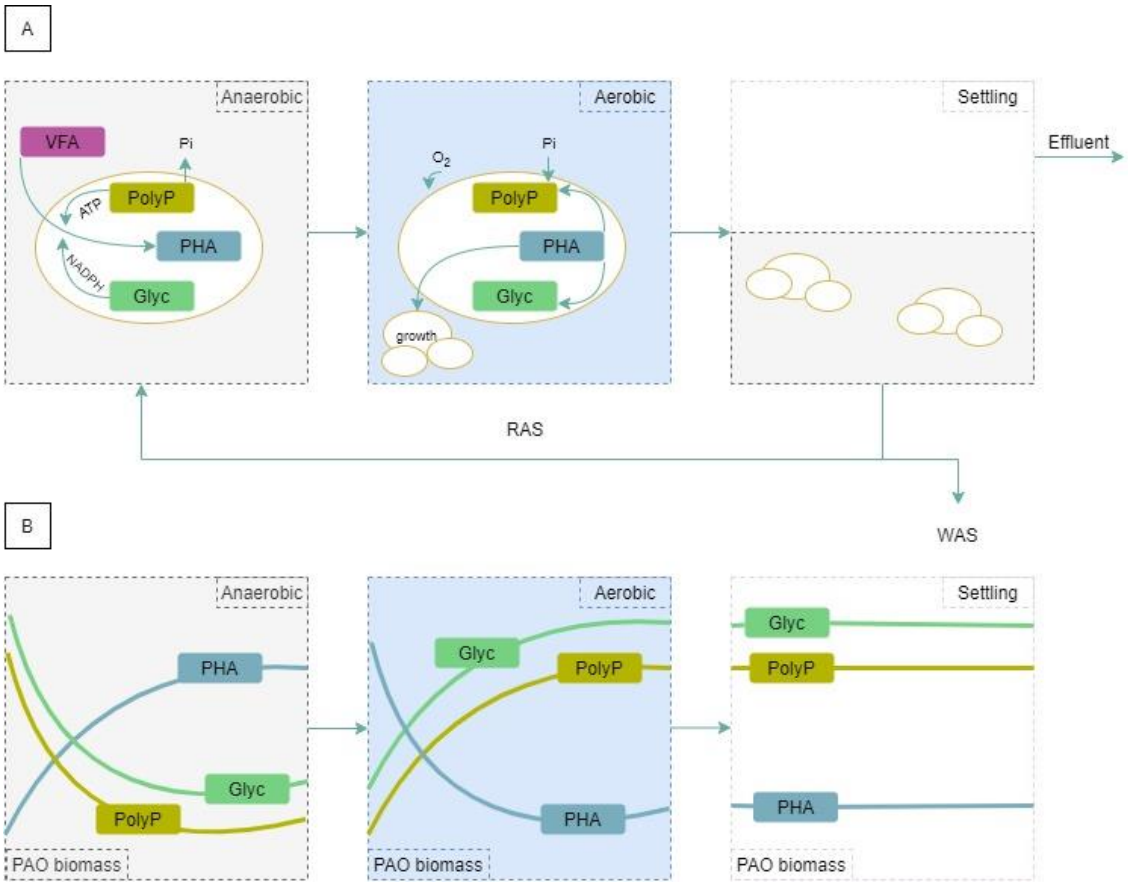

Figure 1 – (A) Schematic diagram of an EBPR process. Representing the three EBPR stages: anaerobic phase (left), aerobic phase (middle), and settling (right). (B) Schematic diagram of the correspondent progression of polymer activity over the three EBPR stages. VFA: volatile fatty acids; PolyP: polyphosphate; PHA: poly-ß-hydroxyalkanoates; Glyc: glycogen; RAS: recycle active sludge; WAS: waste active sludge. Adapted from (van Loosdrecht et al., 2016).

What ensures PAOs a competitive advantage within the EBPR environment, is their capability for rapid substrate uptake in the absence of an electron acceptor, making the carbon source unavailable later on for regular aerobic heterotrophs (da Silva et al., 2019). Other organisms also can survive within this environment such as Glycogen accumulating organisms (GAOs). GAOs have similar behavior to PAOs with the key difference of not producing and consuming polyphosphate. Thus, anaerobically the energy and reducing power for VFA uptake and PHA generation both come from the cleavage of glycogen and/or from the anaerobic operation of the TCA cycle. While aerobically PHA is oxidized resulting in growth and glycogen replenishment (Oehmen et al., 2007). This behavior can also be referred as to Glycogen accumulating metabolism (GAM).

Scientifically there has been a divide regarding the nature of PAOs and GAOs. Some scientific groups defend that GAOs and PAOs are entirely different organisms and perform different metabolic strategies. Whereas others defend that some PAOs and GAOs have the metabolic flexibility to either perform PAM or GAM depending on the

environmental conditions (Schuler & Jenkins, 2003). In this work, PAOs were modeled through a meta-network that both included PAM and GAM, and the predicted metabolism was the one with the best fitness for the environment defined in the model (da Silva et al., 2019).

1.2 – STORAGE METABOLISM

As it was mentioned before, polymers work as carbon and energy reserves, which in turn guarantee a certain level of robustness to the microorganism. Robustness can be defined as the resilience in face of uncertainty. It represents the expected loss of opportunity, which in this case is the opportunity for growth (McPhail et al., 2018). In contrast, efficiency is the best use of resources for a certain goal (growth). Hence, there is a trade-off in resources between directing them to growth (efficiency) or directing them into polymer synthesis (robustness). To guarantee robustness there is a need to synthesize higher amounts of polymers than the optimal (minimal amount necessary for growth). In truth, If PAOs only synthesized the optimal amounts of polymers, glycogen and polyphosphate would be completed degraded in the anaerobic-aerobic switch, and if some change happened, for example, the aerobic phase was longer than usual, PAOs would not have the resources to survive it. This shows that there is a clear balance between the polymers amounts available, survivability/fitness, and growth.

Welles and colleagues tried to investigate this balance by studying the metabolism of an enriched PAOs culture adjusted to different phosphate concentrations in the feed (Laurens Welles et al., 2017). Here, the system was exposed to six increasing phosphate/carbon influent ratios, which led to an increase in polyphosphate and a decrease in glycogen (figure 2).

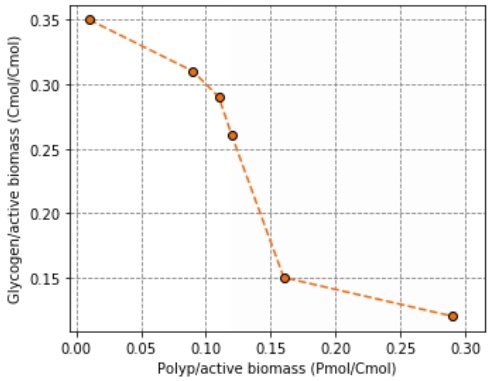

Figure 2 – Experimental work from (Laurens Welles et al., 2017). Experimental polyphosphate and glycogen amount normalized to the amount of active biomass. Each polyphosphate amount was obtained with six increasing phosphate/carbon influent ratios.

Firstly, this shows a clear relation between glycogen and polyphosphate, and that energetically they can be somewhat interchangeable depending on the environmental conditions. Secondly, the decrease in glycogen started stabilizing in the last data point

possibly suggesting a minimum limit for glycogen. A minimum limit for glycogen was also observed in (Zhou et al., 2009) work. In this work, a sludge sample from a PAO enrichment was introduced in a batch reactor and starved in intermittent aerobic-anaerobic conditions. This resulted in a relatively slow phosphorus release and a fast depletion of glycogen. This depletion reached a stable level at approximately 1 mCmol/L, showing that glycogen was never fully depleted.

In addition, Acevedo and colleagues also tried to see this relation between glycogen and polyphosphate and how it ultimately related to the metabolic shift from PAM to GAM (Acevedo et al., 2012). This metabolic shift is often observed when a PAO enrichment is introduced to P-limiting conditions as it was shown in (L. Welles et al., 2016) and (Zhou et al., 2008). Hence, in (Acevedo et al., 2012) work six different levels of polyphosphate were studied, these levels were obtained through starving the system of polyphosphate. Similarly, they showed that reducing the amount of polyphosphate led to the increase in the use of glycolytic reactions in a way to compensate energetically. The shift from PAM to GAM was also observed in the higher PHA production. The increase in the use of glycogen led to the increase in reducing equivalents and acetyl-CoA, which in turn can be reduced for PHA production. Hence, we can see there is a balance between all the internally stored polymers that are highly dependent on environmental conditions.

Finally, da Silva and colleagues investigated this dependency on environmental conditions and how it correlated to metabolic flexibility, including the flexibility to switch from PAM to GAM (da Silva et al., 2020). In their research, they compiled several PAO and GAO literature information. These datasets were plotted against an optimal solution space delimited by three different optimum redox strategies (figure 3). The first redox strategy (figure 3A) used was when there is a little amount of glycogen and the system needs to use the glyoxylate shunt for reducing power; the second (figure 3B) was when all the reducing power is coming from glycogen degradation; the third (figure 3C) was when there is more glycogen than needed and the reductive branch of the TCA cycle is being used to sink electrons, a GAO behavior proposed by (Yagci et al., 2003). The objective of this graph was to see the balance between the amount of glycogen available (and consequently the reducing power available from it) for the reduction of acetate to PHA. Most of the experimental data were within the solution space. As a matter of fact, most of GAO's experimental work was near the third redox strategy delimitation corroborating (Yagci et al., 2003) work. However, there was some article information outside this area especially for PAOs information near the first redox strategy delimitation. This could show that the first redox strategy delimitation is incomplete, and the solution space should be bigger. In truth, in a scenario where there is a little amount of glycogen the system could also obtain reducing power from the partial anaerobic operation of the oxidative branch of the TCA cycle and not only from the operation of the glyoxylate shunt as supported by the works of (D. Brdjanovic et al., 1998);(Louie et al., 2000) and (Yagci et al., 2003). Additionally, this also shows that the balance between PHA and glycogen is not that straightforward and that other polymers are at play. As seen in previous articles, energetically glycogen is also dependent on polyphosphate, so the amount available also plays a role within this balance and in the definition of the solution space. This shows there is a complex balance between the three polymers available and the environment.

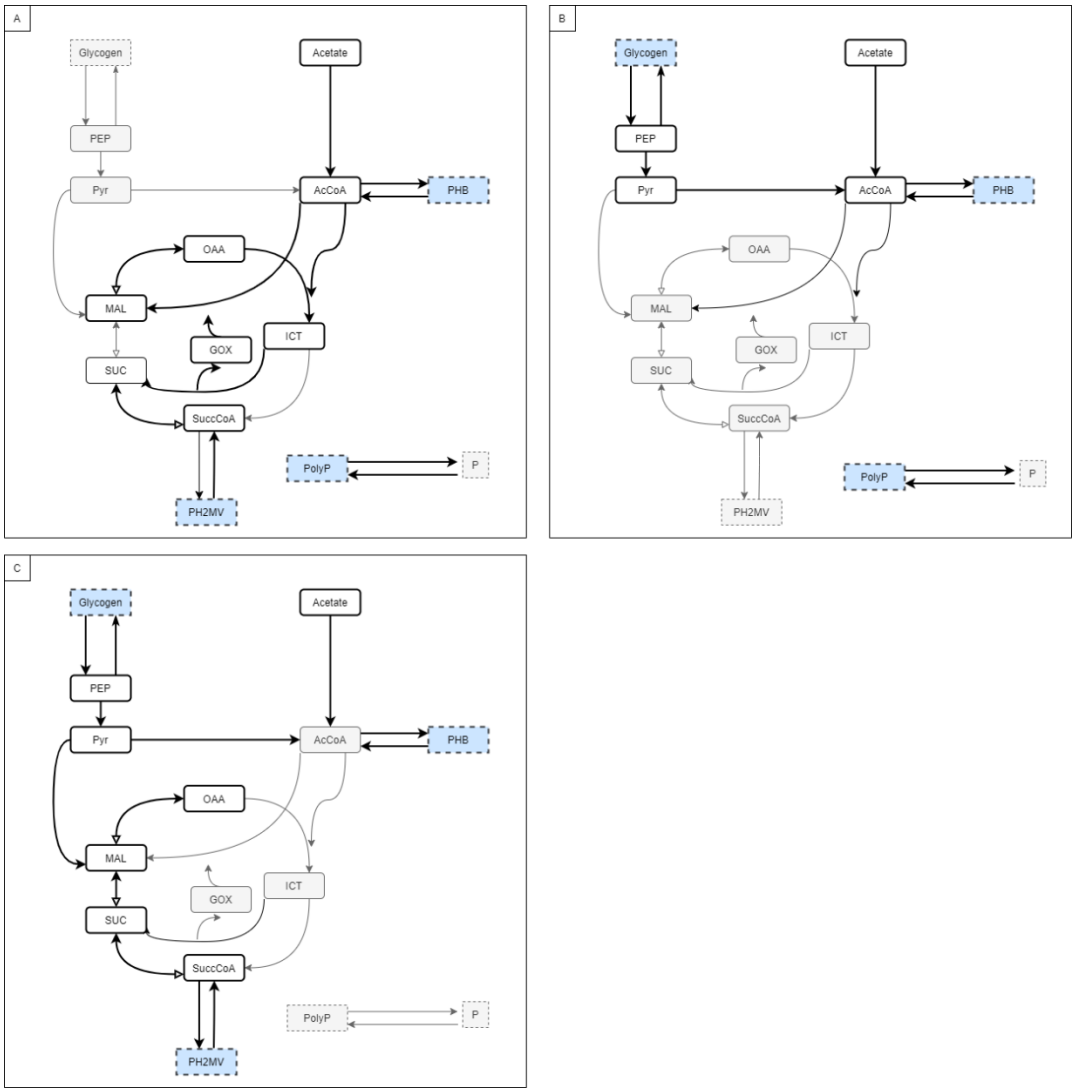

Figure 3 – Different optimum redox strategies for Accumulibacter in anaerobic conditions delimiting the solution space in (da Silva et al., 2020) work. The redox strategies are the following: A) when there is a little amount of glycogen, and the system needs to use the glyoxylate shunt for reducing power. B) all the reducing power is coming from glycogen degradation, C) when there is more glycogen than needed and the reductive branch of the TCA cycle is being used to sink electrons.

1.3- METABOLIC MODELLING

System biology applies the concepts of mathematical analysis and modeling to the study of metabolic networks. It applies a whole system approach to the interactions between metabolites and to the reactions that have been studied previously individually since the observed phenotype results from these interactions. With the rise of genome-scale reconstructions, mathematical systems have been developed to understand and test these reconstructions (Gianchandani et al., 2010). One of the most commonly used approaches is Flux Balance Analysis (FBA).

FBA is a constraint-based model with a linear program (LP) problem approach in which an objective function is maximized or minimized under the constraint of steady-state material balance. This model requires a stoichiometric matrix (S) where the rows represent the metabolites in the model, and the columns the reactions; the reactants for the reactions are represented by a negative value, while the products are represented by a positive value (Gianchandani et al., 2010).

Flux balance analysis has been previously applied to mixed microbial cultures. As matter of fact, Pardelha and colleagues developed a model with the PHA storage reactions and VFA uptake, to investigate the effects of VFA composition in PHA metabolism (Pardelha et al., 2012). This was performed at different time points during the enrichment for a given set of VFA uptake rates, and an accurate prediction of PHA fluxes and PHB/PHV composition was obtained. Additionally, Bordel and colleagues also applied the concepts of FBA to phosphate accumulating organisms (Bordel, 2011). In this work, a metabolic model for PAOs was reconstructed with the metagenomic information from (Martín et al., 2006), and an FBA optimizing was performed for the production of PHA in the anaerobic period. Here it was concluded that the reducing power for PAM was likely to be supplied by glycogen degradation and by the anaerobic operation of the TCA cycle. It is important to highlight that both of these works were only applied to a specific phase of the phosphate accumulating organism cycle.

Notably, a classical FBA works under the assumption of steady-state conditions. FBA provides estimated rates for the whole network under a certain environmental condition rather than time-dependent metabolite concentrations (Perez-Garcia et al., 2016). This assumption of time-invariant metabolism provides a big constraint to this analysis, and it does not always hold. Almost all organisms have some type of variation to their metabolism through time. This is especially true, for organisms that thrive under cyclic environments like photosynthetic organisms (light-dark cycle) and PAOs (anaerobic-aerobic cycle). Conditional flux balance analysis (cFBA) was developed in a way to answer this problem, creating a modeling technique that analyzes the temporal metabolic changes throughout a cycle (Rugen et al., 2015).

This technique was initially developed for phototrophic organisms, more specifically for cyanobacteria. Rugen and colleagues developed this model in order to incorporate the diurnal cycle present in phototrophic metabolism (Rugen et al., 2015). The results obtained from this model were in accordance with the temporal organization of phototrophic metabolism.

Four years later, da Silva and colleagues applied the concept of cFBA to a PAOs meta-network in an anaerobic-feast/ aerobic-famine cycle (da Silva et al., 2019). In this work, the impact of selective pressures on the different storage metabolisms was explored. Different metabolic strategies were observed within the same meta-network by changing the selective pressures. With these results the authors show that certain characteristics are a selective advantage depending on the environment, for example, PAOs have the metabolic advantage of fast acetate uptake in an environment without an external acceptor. The different strategies were PAM, GAM, PHA-AM, and aerobic heterotrophs. These strategies showed a trade-off between robustness and efficiency, PAOs being the most robust and aerobic heterotrophs the most efficient.

The model developed in this work functions as a base model that was further expanded in this thesis. This model is based on the metabolic network of one of the most well studied PAOs, “Candidatus Accumulibacter phosphatis”. The cFBA functions, the metabolic networks, and the model developed can be found in materials and methods (chapter 2.1).

1.4- ENERGY TRADE-OFF IN PAOS POLYMER METABOLISM

Polyphosphate and glycogen polymers work as energy reserves in PAOs metabolism. Where, polyphosphate works as an ATP source, and glycogen as a NADH (and ATP for GAM) source together with the anaerobic operation of the TCA cycle. Depending on the storage polymer amounts available, there is a trade-off between the use of glycogen and polyphosphate that will lead to optimal growth. Which in turn is dependent on the cell's requirements to obtain ATP and NADH for PHA storage. These requirements can be achieved in different amounts depending on the active metabolic routes. This is inherently connected to the fitness that PAM and GAM strategies offer in a certain environment. This thesis aims to determine what is the mechanism controlling this trade-off and if there are limits to this relationship.

To study this concept the following points were explored in this work:

- A phosphate accumulating organism model was constructed and used in a conditional flux balance analysis (cFBA)
    - Initial quotas for the polymers and acetate were calculated through experimental work.
- The energy trade-off between glycogen, polyphosphate, and growth was explored.
- Previous experimental work was compared with the model developed.

2

MATERIALS AND METHODS

2.1- CONDITIONAL FLUX BALANCE ANALYSIS (CFBA) APPROACH

The conditional flux balance analysis (cFBA) assumes a time-variant metabolism. To simulate this, time is subdivided into discrete intervals, making distinct fluxes in each time interval (Rugen et al., 2015). This model includes four main concepts, which are the following:

- **Macromolecules are in a dynamic state whilst intermediates are assumed to be in a quasi-steady state.**

Macromolecules such as proteins and storage polymers were considered time-dependent, whereas intermediates such as ATP and reducing equivalents (modeled here as NADH) were considered to be in a quasi-steady state. This was established under the assumption that transitions with intermediates occur much faster than transitions with macromolecules. So, in this model two groups of metabolites exist, the balanced (in steady-state) and imbalanced metabolites (in dynamic-state) (Rugen et al., 2015). This creates two subsets of the stoichiometric matrix ($\boldsymbol{S_b}$and $\boldsymbol{S_i}$), where the steady state constraint (1) applies to the $\boldsymbol{S_b}$ matrix:

$$\boldsymbol{S_b v^k = 0} \qquad \textbf{(1)}$$

$\boldsymbol{S_b}$ denotes the stoichiometric matrix for the balanced metabolites. While $\boldsymbol{v^k}$ represents the fluxes distribution in the k[th] time interval $k \in \{1,2,\dots,n_t\}$.

- **Dynamic transitions are represented as stable cycles.**

In this model the dynamic conditions were considered a stable cycle, meaning the changes that occurred were consistent and predictable. Therefore, the biomass composition is the same at the beginning and end of the cycle. With this assumption, the final amounts can be defined as a multiple of the defined initial amounts:

$$\boldsymbol{M(t_{end}) = \propto M(t_{start})} \qquad \textbf{(2)}$$

Where $\boldsymbol{M}$ denotes the imbalanced compound amounts at the final time-step ($\boldsymbol{t_{end}}$) and at the start of the cycle ($\boldsymbol{t_{start}}$), and ∝ the foldchange**.**

Growth can be defined by the foldchange (α) and the whole system can be optimized for the highest value of α.

According to equation (2), the foldchange is highly affected by $M(t_{start})$. To control this influence over α a weight matrix ($\boldsymbol{w^T}$) can be defined, where each position represents a weight for a specific metabolite over $M(t_i)$.

$$\boldsymbol{w^T M(t_{start}) = 1} \quad \textbf{(3)}$$

In this work, the weight matrix is used to normalize the system to 1 g of dry biomass.

- **Compounds can have an inherent quota.**

Quotas in this model are introduced in a way to constrain imbalanced metabolites over the cycle. These quotas are always applied to inert compounds, such as biomass precursors and non-catalytic proteins, in a way to ensure their synthesis. So, a minimum quota in all time-points is introduced for these compounds:

$$\boldsymbol{B^k_{quota} M^k \geq C^k_{quota}} \quad \textbf{(4)}$$

Where B^k_{quota} is an index matrix and C^k_{quota} is the quota value. This is applied for each time point for the compound amount matrix M^k $k \in \{1,2,\dots,n_t\}$.

Additionally, this quota feature can be used on other imbalanced metabolites to ensure specific behaviors. Therefore, other quota types were defined within this model, such as :

Minimal initial quota

$$\boldsymbol{B^i_{quota} M^i \geq C^i_{quota}} \quad \textbf{(5)}$$

Initial quota

$$\boldsymbol{B^i_{quota} M^i = C^i_{quota}} \quad \textbf{(6)}$$

Maximal quota for a specific time point

$$\boldsymbol{B^{x}_{quota} M^{x} \leq C^{x}_{quota}} \quad \textbf{(7)}$$

Where x represents the specific time point.

- **Fluxes can be constrained by enzyme levels.**

In cFBA, the flux through a metabolic reaction can be constrained by the enzyme amount with its capacity constraint:

$$\boldsymbol{A^{k}_{cap} v^{k} \leq B^{k}_{cap} M^{k-1}} \quad \textbf{(8)}$$

Where A^{k}_{cap} is a matrix with the enzyme capacity values (inverse kcats), B^{k}_{cap} is the index matrix and v^{k} is the flux distribution for $k \in \{1,2,\dots,n_t\}$.

It is important to note enzyme capacities were not introduced in the model developed in this work.

In addition, this model also applies the constraint that compound amounts cannot be negative.

$$\boldsymbol{M^{k} \geq 0} \quad \textbf{(9)}$$

And it also constraints the fluxes to an upper and lower bound:

$$\boldsymbol{b_{low} \leq v_{k} \leq b_{up}} \quad \textbf{(10)}$$

With all these constraints the model performs a global optimization for α through a linear problem (LP).

2.2 – MODEL CONSTRUCTION AND IMPLEMENTATION

All model simulations were implemented in *Python 3.7.3* in a *Jupyter notebook* environment as a linear optimization problem (figure 4). This optimization problem was solved with the support of the *Python* package *optlang* with the *GLPK* solver.

Data: optimization Problem $P(\alpha)$, ϵ
Result: maximal biomass fold change α
$\alpha = 1$
while *where exists a solution to* $P(2\,\alpha)$ **do**
  $\alpha = 2\,\alpha$
end
$\Delta\alpha = \alpha/2$
while $\Delta\alpha > \epsilon$ **do**
  if *where exists a solution to* $P(\alpha + \Delta\alpha)$ **then**
    $\alpha = \alpha + \Delta\alpha$
  end
  $\Delta\alpha = \Delta\alpha/2$
end

Figure 4 – Linear optimization algorithm to identify the highest foldchange (α) with the precision of ϵ (Rugen et al., 2015).

This model runs from 0 to 5 hours in time discretization of 1. The anaerobic time-span was of two hours and the anaerobic time-span was three hours.

2.2.1 – METABOLIC NETWORK

As it was mentioned before, the developed metabolic network was based on the metabolic model used in (da Silva et al., 2019) work. The key difference between the model developed in (da Silva et al., 2019) and the model developed in this work (figure 5) is the expansion of the TCA cycle reactions. The introduced reactions were based on the following genome database (*KEGG GENOME T00966*, n.d.) for “Candidatus Accumulibacter phosphatis”. The original model can be found in the supplementary information (figure S9). It's important to note, that in this thesis enzyme capacities were not used, instead, general enzyme and ribosome synthesis reactions were implemented.

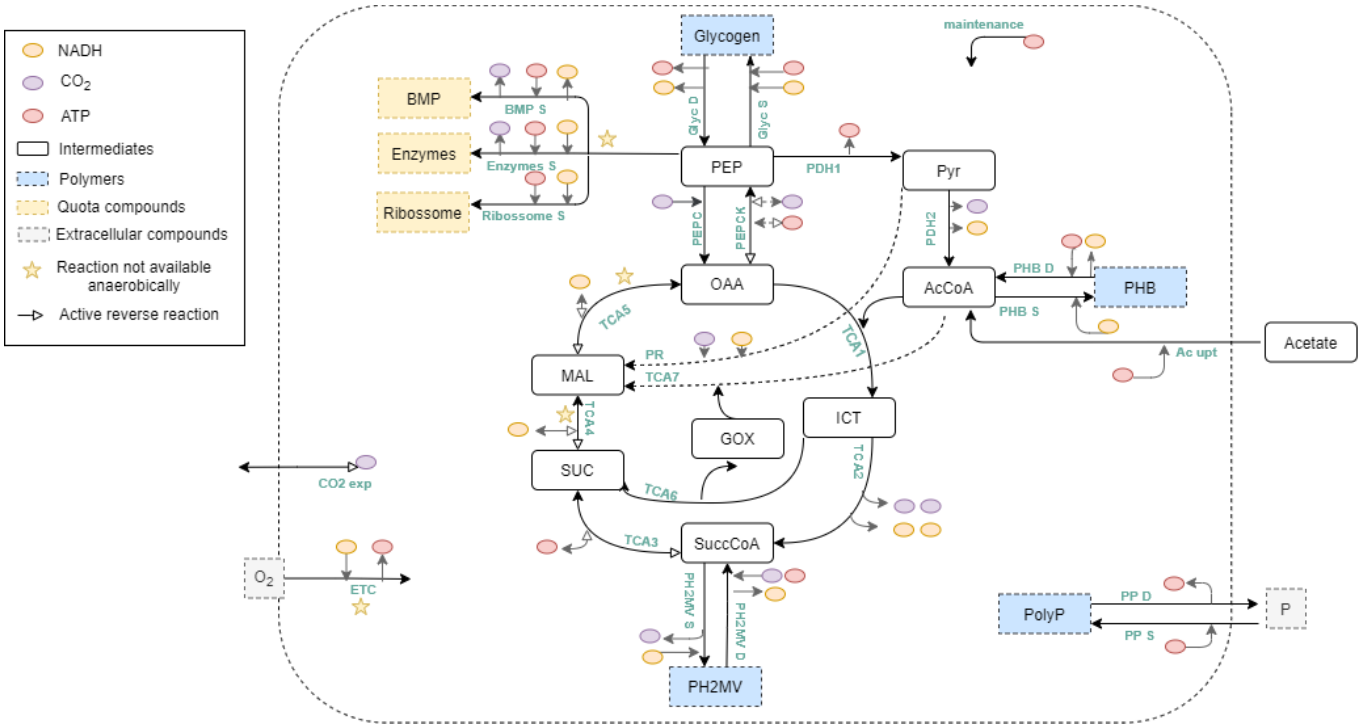

Figure 5 - Representation of the metabolic model. Meta-network for Phosphate accumulating organism developed in this work, based on the simplified metabolic network of "Candidatus Accumulibacter phosphatis". Glyc D, S: glycogen degradation and synthesis reactions; BMP S: Biomass precursors synthesis reaction; Enzymes S: general enzymatic synthesis reaction; Ribosome S: general ribosome synthesis reaction; PDH 1,2: pyruvate dehydrogenase reactions; PEPC: Phosphoenolpyruvate formation reaction; PEPCK: Phosphoenolpyruvate carboxykinase reaction; PHB D, S: PHB degradation and synthesis reaction; Ac up: Acetate uptake reaction; TCA 7,5: glyoxylate shunt; TCA 1,2: oxidative branch of the TCA cycle; TCA 3,4,5: reductive branch of the TCA cycle; PH2MV D, S: PH2MV degradation and synthesis reaction; ETC: electron transport chain; CO_2 exp: CO_2 export reaction; PP D, S: polyphosphate degradation and synthesis; PR: conversion of pyruvate to malate reaction.

In order to construct a stoichiometric matrix (S) for the model, a complete list of every reaction and respective stoichiometry in the system is needed (Table 1). In a cFBA system the stochiometric matrix (S) is further divided into a balanced stoichiometric matrix ($\boldsymbol{S_b}$) and an imbalanced stoichiometric matrix ($\boldsymbol{S_i}$). In this case, the balanced metabolites were Acetyl-CoA (AcCoA), Succinyl-CoA (SuccCoA), CO_2, Phosphoenolpyruvate (PEP), Oxaloacetate (OAA), isocitrate (ICT), Succinate (SUC), malate (MAL), glyoxylate (GOX), pyruvate (Pyr), ATP, and NADH. The imbalanced metabolites were Acetate (Ac), PHB, PH_2MV, glycogen (Glyc), polyphosphate (PP), biomass precursors (BMP), Enzymes, and Ribosomes.

Table 1 – Complete reaction list used in the metabolic network; this information is used to construct a stoichiometric matrix (S).

Reaction	Stoichiometry	Description	
Ac_upt	$Ac + 1ATP \rightarrow AcCoA$	Uptake of external acetate.	**(11)**
Glyc S	$2PEP + 2ATP + 2NADH \rightarrow Glyc$	Glycogen synthesis.	**(12)**
Glyc D	$Glyc \rightarrow 2PEP + ATP + 2NADH$	Glycogen degradation.	**(13)**
PEPC	$PEP + CO_2 \rightarrow OAA$	Phosphoenolpyruvate formation.	**(14)**
PEPCK	$OAA + ATP \leftrightarrow PEP + CO_2$	Phosphoenolpyruvate carboxykinase.	**(15)**
BMP S	$0.635PEP + 1.065ATP \rightarrow BMP + 1.2075NADH + 0.905CO_2$	Biomass precursors synthesis	**(16)**
Enzyme S	$15.48PEP + 124.45ATP + 65.768NADH \rightarrow Enzyme + 1.483CO_2$	General enzyme synthesis.	**(17)**
Ribosome S	$11.604PEP + 44.038ATP + 51.657NADH \rightarrow Ribossome$	General ribosome synthesis.	**(18)**
PHB S	$2AcCoA + NADH \rightarrow PHB$	PHB synthesis.	**(19)**
PHB D	$PHB + 2ATP \rightarrow 2AcCoA + NADH$	PHB degradation.	**(20)**
PH_2MV S	$2SuccCoA + NADH \rightarrow PH_2MV + 2CO_2$	PH_2MV synthesis.	**(21)**
PH_2MV D	$PH_2MV + 2CO_2 + 2ATP \rightarrow 2SuccCoA + NADH$	PH_2MV degradation.	**(22)**
PP S	$1.26ATP \rightarrow PP$	Polyphosphate synthesis.	**(23)**
PP D	$PP \rightarrow ATP$	Polyphosphate degradation.	**(24)**
ETC	$NADH \rightarrow 1.85ATP$	Electron transport chain.	**(25)**
CO_2 exp	$CO_2 \leftrightarrow$	CO_2 export.	**(26)**
Vcomp	$Ac \rightarrow$	Competition acetate uptake for “leftover” acetate.	**(27)**
Maintenance	$ATP \rightarrow$	Maintenance reactions	**(28)**
Ac feed	$\rightarrow Ac$	Fake replenishment acetate reaction to close the cycle.	**(29)**
TCA1	$AcCoA + OAA \rightarrow ICT$	Conversion of Oxaloacetate to Isocitrate in the TCA cycle.	**(30)**
TCA2	$ICT \rightarrow SuccCoA + 2NADH + 2CO_2$	Conversion of Isocitrate to Succinyl- CoA in the TCA cycle.	**(31)**
TCA3	$SuccCoA \leftrightarrow ATP + SUC$	Conversion of Succinyl-CoA to succinate in the TCA cycle.	**(32)**
TCA4	$SUC \leftrightarrow MAL + NADH$	Conversion of Succinate to Malate in the TCA cycle.	**(33)**
TCA5	$MAL \leftrightarrow OAA + NADH$	Conversion of Malate to oxaloacetate in the TCA cycle.	**(34)**

TCA6	$ICT \rightarrow GOX + SUC$	Conversion of isocitrate to succinate in the glyoxylate shunt.	**(35)**
TCA7	$AcCoA + GOX \rightarrow MAL$	Conversion of Acetyl-CoA to malate in the glyoxylate shunt.	**(36)**
PR	$Pyr + NADH + CO_2 \rightarrow MAL$	Conversion of pyruvate to malate in pyruvate metabolism.	**(37)**
PDH1	$PEP \rightarrow Pyr + ATP$	Pyruvate dehydrogenase.	**(38)**
PDH2	$Pyr \rightarrow AcCoA + CO_2 + NADH$	Pyruvate dehydrogenase.	**(39)**

Reaction constrains

In addition, reactions were further restricted by lower and upper bounds (Table 2). All reactions, with some exceptions, were restricted at all time points with an upper bound of 1000 mCmol/g_{dw}/h, in a way to represent an infinite number, and a lower bound of 0 mCmol/g_{dw}/h. In the last time-point, all reactions had an upper bound of 0 mCmol/g_{dw}/h except for Ac feed that had an upper bound of a 1000 mCmol/g_{dw}/h (in the other time points this reaction had an upper bound of 0 mCmol/g_{dw}/h), in a way to replenish the carbon pool. Reverse reactions such as TCA3,4,5, PEPCK, and CO_2 export had a lower bound of -1000 mCmol/g_{dw}/h.

To represent the aerobic/ anaerobic cycle the ETC reaction was only active aerobically. Hence, the defined upper bound for this reaction was 1000 in the aerobic time-span and 0 in the anaerobic time-span (table 2).

Other reactions were also only active aerobically (marked in figure 5 by a star), such as TCA4 and in some simulations TCA5. The synthesis reactions for inert compounds (BMP, Enzyme, and Ribosome) were also only active anaerobically, in a way to limit growth to the anaerobic phase (table 2).

In this network, the metabolites GTP and $FADH_2$ were not represented and assumed to be comparable to ATP and NADH, respectively. The maintenance flux was set to a constant value of 0.03 mmol ATP/(g_{dw}h) in both the upper and lower bound this was calculated based on experimental work (figure S1- chapter 7.1).

Table 2 – Summary table of the upper and lower bounds introduced to the metabolic reactions. In green it's possible to see maximal upper bound applied (1000 mCmol/g_{dw}/h), In grey the bound of 0 mCmol/g_{dw}/h, in red the lowest lower bound applied (-1000 mCmol/g_{dw}/h), and in yellow the fixed amount for maintenance.

reaction fluxes (mCmol/gdw/h)	bound	Anaerobic		Aerobic		
		1 h	2 h	3 h	4 h	5 h
PEPCK, CO_2 export, TCA3, (and in some simulations TCA5)	upper	1000	1000	1000	1000	0
	lower	-1000	-1000	-1000	-1000	0
TCA4 (and in some simulations TCA5)	upper	0	0	1000	1000	0
	lower	-1000	-1000	-1000	-1000	0
ETC, BMP S, Enzyme S, Ribosome S	upper	0	0	1000	1000	0
	lower	0	0	0	0	0
maintenance	upper	0.03	0.03	0.03	0.03	0
	lower	0.03	0.03	0.03	0.03	0
Ac feed	upper	0	0	0	0	1000
	lower	0	0	0	0	1000
Other reactions	upper	1000	1000	1000	1000	0
	lower	0	0	0	0	0

Metabolite constrains

Metabolites were also restricted with the use of quotas. To ensure the synthesis of inert compounds, BMP, enzymes, and ribosomes were given minimum quotas at all time points. Additionally, polymers (glycogen, polyphosphate, PHB, and PH_2MV) and acetate were given initial quotas (table 3) following experimental work. Acetate was also given a quota of 0 mCmol/g_{dw} at the switch between aerobic and anaerobic, in a way to guarantee that the carbon source is fully consumed anaerobically, and in turn, guarantee that the acetate uptake is representative of PAOs behavior.

In this work, simulations were performed to study the influence of environmental changes in polymer metabolism in growth, especially in the energy trade-off between glycogen and polyphosphate. In order to simulate these changes in polymers, the concept of quotas was used.

cFBA uses quotas in a way to constrain imbalance metabolites to a certain value over the cycle. Quotas are categorized in four different ways: minimal initial quotas, initial quotas, minimal quotas for all time points, and quotas for specific time points.

All simulations had quotas for all time points for inert compounds (BMP, enzyme, and ribosome) with a value of 0.183 mCmol/g_{dw}. This value was based on the work from (da Silva et al., 2019). Additionally, in every simulation acetate had an initial quota, that defined a certain feeding value, and a quota of 0 mCmol/g_{dw} for the end of the anaerobic phase (t=2h), in a way to constrain the acetate uptake.

Finally, simulations had polymer initial quotas (polyphosphate, glycogen, PHV, and PH2MV) based on experimental work that could also vary between a range (table 3). In a way to create comparable results to experimental amounts and to simulate different environmental conditions. In the following table, is possible to see the initial quotas used in each simulation.

Table 3 – Summary table of the initial quotas used in each simulation performed in this work. In all simulations, BMP, ribosomes, and enzymes had a set minimal quota of 0.183 mCmol/gDW at all time points; and acetate had a maximum quota of 0 mCmol/gDW at time point 2.

	Initial quotas				
mC(P)mol/g_{dw}	Ac	PP	Glyc	PHB	PH2MV
Reference quotas	3.84	0.37	3.92	0.65	1.03
Polyphosphate vs. Glycogen quotas	3.84	from 0 to 10	0,0.25,0.5,0.75,1	0.65	1.03
Acetate vs. Polyphosphate quotas Present in supplementary information chapter 7.3.2	from 0 to 10	0,1,2,3	3.92	0.65	1.03
Acetate vs. Glycogen quotas Presente in suplementar information chapter 7.3.3	from 0 to 10	0.37	0,1,2,3	0.65	1.03

The reference quotas were retrieved and calculated from experimental work described in chapters 2.3 and 7.1. These quotas were used to fix initial polymer amounts and

acetate to a certain value and were calculated experimentally through the SBR operation and polymer determination.

2.3 – EXPERIMENTAL WORK

2.3.1 – SBR OPERATION

A PAO and GAO enrichment was obtained through the operation of a sequencing batch reactor (SBR). The SBR was operated and controlled by an Applikon controller using BioXpert software. The SBR was operated in the following cycle (table 4).

Table 4 – SBR phases and time over a 6h EBPR cycle.

Phase	**Time (min)**
Feed	30
Anaerobic	105
Aerobic	134
Sludge	1
Settling	70
Effluent	20
Cycle	360

The reactor had a volume of 1.5 L and each cycle fed 0.750 L of the synthetic substrate. The pH was controlled by dosing 1 M HCL and 1 M NaOH and the anaerobic /aerobic phases were simulated by sparging nitrogen gas and compressed air, respectively. The reactor was mixed with an 800 rpm speed. The SBR was controlled at a biomass retention time (SRT) of 8 days and a hydraulic retention time (HRT) of 12 h.

The concentrated medium was prepared with and diluted with demineralized water. Each cycle was fed with 600 ml of demineralized water and 75 ml of mineral solution and COD medium. The mineral medium contained per liter : 1.524 g/L NH_4Cl, 1.586 g/L $MgSO_4 \cdot 7H_2O$, 0.4 g/L $CaCl_2 \cdot 2H_2O$, 0.48 g/L KCL, 0.04 g/L N-allylthiourea, 2.22 g/L $NaH_2PO \cdot H_2O$, 0.04 g/L yeast extract and 6 ml/L of trace elements. The COD medium contained per liter: 40.62 mM $CH_3COONa*3H_2O$, and 12.5 mM $C_3H_5NaO_2$.

2.3.2 – TSS AND VSS CALCULATIONS

To determine TSS (total suspended solids) and VSS (volatile suspended solids) from the bioreactor, samples were collected *in situ* into 15 ml falcon tubes. These samples were centrifuged for 5 minutes at 4000 g and then decanted. Tap water was added to the pellet and the samples were resuspended (vortex) and centrifuged and decanted

again with the same conditions. The centrifuged used was the multifuge 1 L-R model by Heraeus.

To determine the TSS amount, the sampled biomass was added to a pre-dried aluminum tray. This tray was then added to a stove (model function line by Heraeus) at 105 ºC the samples were dried overnight and afterward weighted.

$$\boldsymbol{TSS = \frac{Tray\ after\ stove - Empty\ dry\ tray}{initial\ sample\ weight}} \quad \textbf{(40)}$$

To determine the VSS amount, the aluminum trays containing the samples were added into a furnace at 550 ºC (carbolite model) for 3h. Afterward, the tray was weighted.

$$\boldsymbol{VSS = \frac{Tray\ after\ stove - tray\ after\ furnace}{initial\ sample\ weight}} \quad \textbf{(41)}$$

In this work, the resulting TSS was 1.7 ± 0.04 g/L while the VSS was 1.51 ± 0.005 g/L, samples were retrieved at the anaerobic-aerobic switch in duplicate form.

2.2.3 – ORTHOPHOSPAHTE MEASUREMENT AND POLYPHOSPHATE DETERMINATION

The polyphosphate amount was indirectly calculated through the orthophosphate (PO_4) concentration in the reactor bulk liquid. This concentration was measured by *in situ* sampling. Each sample was filtered through 0.45 µm size pore filters and collected into 2 ml Eppendorf. The orthophosphate concentration was determined using a discrete analyzer (DA) model gallery by thermo scientific. The polyphosphate amount was calculated each time point by subtracting the orthophosphate amount to the highest phosphate release with the sum of the TSS-VSS difference.

$$\boldsymbol{PolyP = \left[PO_{4\ max} - PO_{4\ i}\right] + [TSS - VSS]} \quad \textbf{(42)}$$

Where $PO_{4\ max}$ represents the maximal orthophosphate concentration obtained (concentration at the aerobic-anaerobic switch) and $PO_{4\ i}$ the orthophosphate concentration for a specific time point in the cycle ($_i$).

2.2.4 – PHA DETERMINATION

Samples were collected *in situ* from the reactor into 15 ml falcon tubes. These tubes contained 4-5 drops of paraformaldehyde (37%) which were added before sampling in a fume hood, this was done to stop biomass activity in the sample. To remove the liquid phase, the samples were centrifuged for 15 minutes at 4500 rpm and the supernatant was removed by decanting. Then tap water was added and the samples were resuspended (vortex) and centrifuged and decanted again with the same conditions. Afterward, the samples were pre-frozen at -80 ºC for 2 hours and freeze-dried at -80 ºC at 0.1 mbar overnight. The centrifuged used was the multifuge 1 L-R model by Heraeus and the freeze drier used was model Alpha 1-4 LDplus, Crist.

For PHB and PHV determination, 15 to 30 mg of freeze-dried sample was added to a glass tube together with 50 µl of PHB internal standard. The PHB internal standard consists of a dilution of 1 mg benzoic acid in 1-propanol. Then 1.5 ml of dichloroethane and 1.5 ml of concentrated HCL with 1-propanol (1:4 in volume) was added to each tube. Samples are digested and esterified for 3 hours at 100 ºC in a heat block (model SBH200D by Stuart). During these 3 hours, the tubes were vortexed every 30 min to ensure that the sample was homogeneous. After cooling to room temperature to extract the free acids 3 ml of milli-Q water was added and then the tubes were mixed with the vortex. After mixing, to separate the organic from the aqueous phase, the sample was centrifuged for 15 minutes at 2500 rpm. Afterward, using filtered tips 1 ml of the sample was removed and filtered into gas chromatography vials (GC vials). Finally, using a gas chromatography model 6890N, Agileny, U.S.A equipped with an FID, on an HP Innowax column the esters formed were analyzed, and the internal PHB and PHV concentrations were calculated. This protocol was based on (Smolders et al., 1994) work.

2.2.5 – GLYCOGEN DETERMINATION

Samples were collected *in situ* from the reactor into 15 ml falcon tubes. These tubes contained 4-5 drops of paraformaldehyde (37%) which were added before sampling in a fume hood, this was done to stop biomass activity in the sample. To remove the liquid phase, the samples were centrifuged for 10 minutes at 4500 rpm and the supernatant was removed by decanting. Then tap water was added and the samples were resuspended (vortex) and centrifuged and decanted again with the same conditions. Afterward, the samples were pre-frozen at -80 ºC for 2 hours and freeze-dried at -80 ºC at 0.1 mbar overnight.

For glycogen determination, around 5 mg of biomass were measured into glass tubes and 5 ml of 0.9 M of HCL were added. These samples were vortexed and digested for 5 hours at 100 ºC in a heating block (model SBH200D by Stuart). Every hour the tubes were vortexed to homogenize the samples. After cooling down to room temperature the samples were filtered using 0.45 µm pore size filters. Finally, the glucose concentration of each digested sample was analyzed through the Sigma Aldrich glucose (GO) assay kit, GAGO20-1KT.

3

RESULTS

3.1 – ANALYSIS OF THE METABOLIC MODEL

3.1.1 -SIMULATION WITH REFERENCE INITIAL QUOTAS

A typical EBPR cycle was simulated with the metabolic model described in chapter 2.2. The cycle ran for 5 h in time discretization of 1 hour, where the first 2h represent the anaerobic phase and the last 3 h the aerobic phase. In this model, growth is represented by foldchange (α), due to the assumption that the final amounts can be defined as a multiple (α) of the defined initial amounts, hence, at α =1 there is no growth. With the use of quotas, acetate was constrained to be consumed within 1 hour of the simulation, and polymers were constrained to specific initial amounts based on experimental data (table 3 -reference quotas). With these constraints, an LP optimization was performed (figure 6). In Addition, the model results were compared with the experimental data obtained through the reactor operation and polymer determination described in chapter 2.3. Additional information about the experimental amounts can be found in the supplementary information (chapter 7.1.2).

We can see in figure 5, that the model simulation results (full lines) present a PAM-like behavior. The PHA polymers (PHB and PH_2MV) are synthesized in the anaerobic phase functioning as a carbon storage polymer and are consumed in the aerobic phase for glycogen, polyphosphate, and biomass synthesis. In turn, glycogen and polyphosphate are consumed in the anaerobic phase functioning as energy and reducing power sources. This modeled behavior generates comparable amounts to the amounts observed experimentally (dotted lines), suggesting that the model created is comparable to reality. The observed experimental values were obtained through an SBR operation controlled with a sludge retention (SRT) time of 8 days. Taking into account that the foldchange obtained in the model simulation was 1.046 and that the model is normalized for 1 g_{dw}/L of biomass it's possible to calculate a comparable SRT value of 10.8 days for the modeled results (assuming that the biomass produced is removed at the end of the cycle).

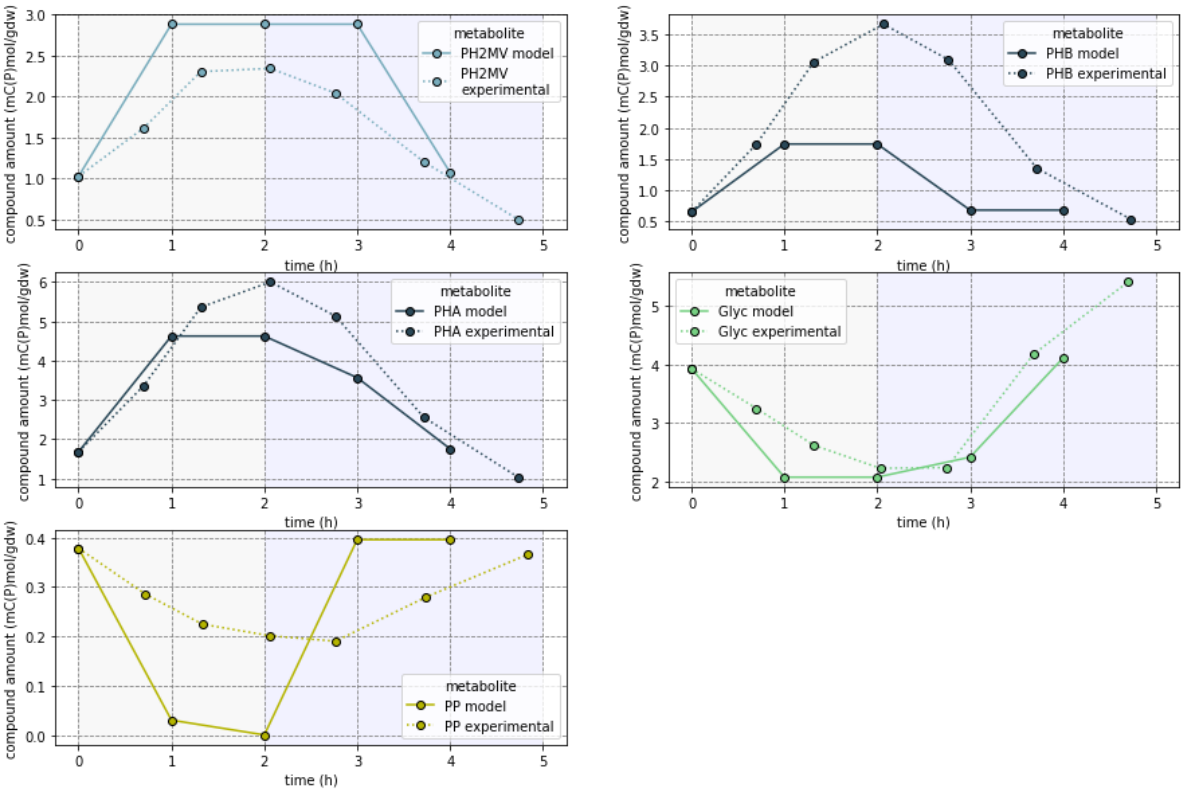

Figure 6 - Metabolic concentrations of polymers through time in a cFBA simulation (model – full lines) and SBR operation (experimental – dotted lines) in an EBPR system. The first 2h represent the anaerobic time and the last 3h the aerobic time. For the model results, the initial quotas used can be found in table 3 (reference quotas) and the complete reactions and model restrictions can be found in chapter 2.2, the resulting foldchange was 1.046. For the experimental results, the reactor operation and polymer determination information can be found in chapter 2.3.

3.1.2 – SIMULATION WITH VARIED INITIAL QUOTAS FOR POLYPHOSPHATE AND GLYCOGEN

To understand the relationship between the use of glycogen and polyphosphate and how it relates to growth, multiple simulations were performed with the model created and validated by experimental work (Figure 6). In these simulations, polyphosphate and glycogen initial quotas were set to different amounts, whilst PHA and acetate initial quotas were set to the same amounts throughout all simulations (polyphosphate vs. glycogen quotas – table 3). Each simulation was performed to a typical EBPR cycle with the metabolic model described in chapter 2.2, where the cycle ran for 5 h in time discretization of 1 hour, the first 2h represent the anaerobic phase, and the last 3 h the aerobic phase. The generated foldchange (α) in each simulation was compared in figure 7. In this model, growth is represented by foldchange (α), due to the assumption that the final amounts can be defined as a multiple (α) of the defined initial amounts.

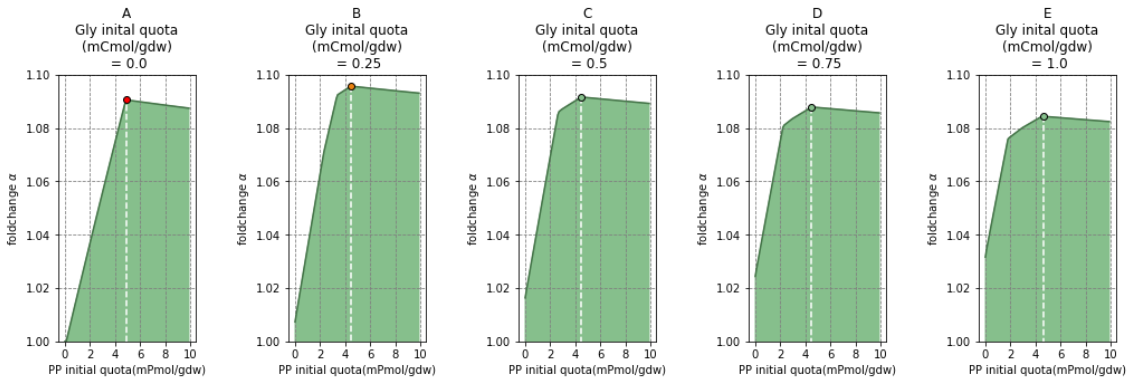

Figure 7 – Variation of foldchange (α) vs. a range of fixed initial polyphosphate (PP) and glycogen (Gly) quotas. Achieved through the performance of multiple simulations in an EBPR system where the first 2h represent the anaerobic time and the last 3h the aerobic time. Each simulation was performed with different polyphosphate (PP) initial quotas [from 0 to 10 mPmol/g_{dw}] at different fixed glycogen (Glyc) initial [0,0.25,0.5,0.75,1 mCmol/g_{dw} in steps of 0.1] resulting in a specific foldchange. Other fixed quotas used in these simulations can be found in table 3 (polyphosphate vs. glycogen quotas).In each graph, the highest foldchange achieved is highlighted by a marker.

The results indicate a relation between glycogen and polyphosphate for organisms living under the simulated conditions. All graphs have a similar profile, where the foldchange increases with the increase of polyphosphate initial quota, for each glycogen initial quota simulation (figure 7A, 7B, 7C, 7D, and 7E), until it reaches an upper limit and starts to slightly decline. In simulations, 7B, 7C, 7D, and 7E this increase is shaped in two stages, where the first stage is observed to have a sharper slope which is followed by a second stage with a slower increase until it reaches the upper limit.

These two different stages represent a shift in the source of reducing power. To illustrate this shift, the specific metabolic fluxes for NADH production were plotted for two distinct points in these two stages for simulation 6B (figure 8). In the first stage (figure 8B), it's possible to see that the source reducing power (NADH) is coming from glycogen degradation (Glyc_D) and the operation of the TCA2 reaction (Conversion of Isocitrate to Succinyl- CoA). Whilst, in the second stage the reducing power is coming from glycogen degradation, the TCA2 reaction, and the TCA5 reaction (conversion of malate to oxaloacetate) (figure 8C). The use of the TCA5 reaction for reducing power represents a shift in the metabolic routes used. With the increase of the initial polyphosphate amount, more ATP is being produced through polyphosphate degradation, in turn, glycogen degradation also produces ATP. Therefore, at a certain point, the organism starts to rely more on the TCA cycle to generate NADH than on glycogen degradation (switch between phases), In order to avoid overproducing ATP. Hence, the organism switches from using the reducing branch of the TCA cycle (figure 8D) and starts using the glyoxylate shunt to produce NADH through TCA5 (figure 8E). At the same time, ATP is being consumed in the reverse reaction of TCA3 (Conversion of succinate to Succinyl-CoA) for both stages (ATP sink).

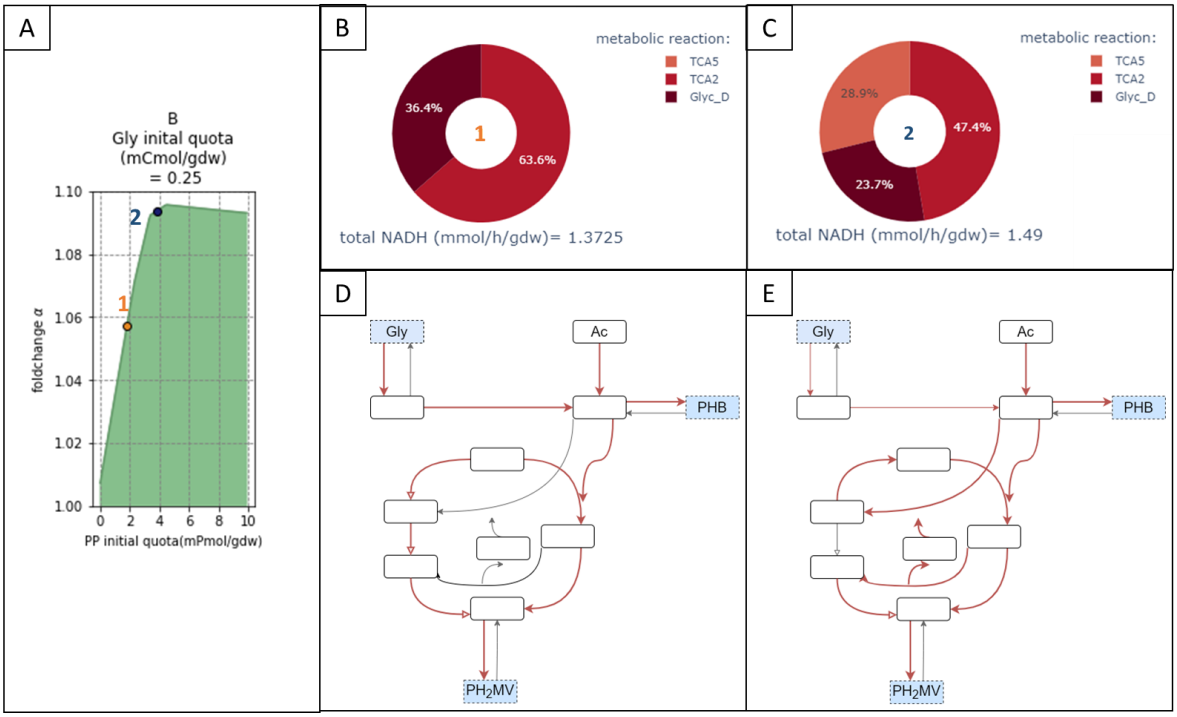

Figure 8 - Investigation of the NADH sources for two simulations (1A, 2A) in the different increasing stages for a fixed glycogen initial quota of 0.25 mCmol/gdw (A), and a polyphosphate initial quota of 1.8 mPmol/gdw (1A) and 3.8 mPmol/gdw (2A), respectively. These simulations were performed in an EBPR system where the first 2h represent the anaerobic time and the last 3h the aerobic time. Other polymer and acetate were fixed with quotas according to table 3. B) Specific metabolic fluxes for NADH production in the anaerobic phase for simulation 1A. C) Specific metabolic fluxes for NADH production in the anaerobic phase for simulation 1B. D) Simplified metabolic route employed by simulation 1A in the anaerobic phase. Pathways highlighted in grey are not active and pathways highlighted in red are active. E) Simplified metabolic route employed by simulation 1B in the anaerobic phase. Pathways highlighted in grey are not active and pathways highlighted in red are active. Pathways that are highlighted in red with a smaller width, represent pathways that are less active in reference to the previous metabolic route (D). Glyc_D: glycogen degradation; TCA2: conversion isocitrate to Succinyl-CoA in the TCA cycle; TCA5: conversion of malate to oxaloacetate in the TCA cycle.

The upper limits observed in each simulation in figure 7 represent optimal growth for the given glycogen initial quota. Hence, higher polyphosphate amounts from the optimal will lead to a slight decline in foldchange, due to resources being overspent towards the production of stored polyphosphate. In the first two graphs (7A and 7B), it is possible to observe an increase in this upper limit (a higher foldchange is achieved), whereas in the last three graphs (7C, 7D, and 7E) a decrease in the maximal foldchange achieved is observed. This indicates an optimal initial glycogen amount of 0.25 mCmol/g_{dw} within this simulation.

Simulation 7A indicates that it is possible to grow without glycogen. To the extent of our knowledge, growth with full depletion of glycogen has never been reported in PAOs literature. Therefore, growing without glycogen might not be a possible PAOs behavior. Glycogen together with the anaerobic operation of the TCA cycle represents a source of reducing power for PAOs. Knowing that simulation 7A shows growth without a source of

glycogen, the reducing power must come fully from the TCA cycle. This might suggest an overestimation of the TCA cycle in the developed model. To test this hypothesis the specific metabolic fluxes for NADH production for both a simulation of the maximal foldchange quotas at glycogen 0.25 mCmol/g_{dw} (Figure 7B – orange marker) and with the maximal foldchange quotas at glycogen 0 mCmol/g_{dw} (Figure 7A – red marker) were plotted (figure 9).

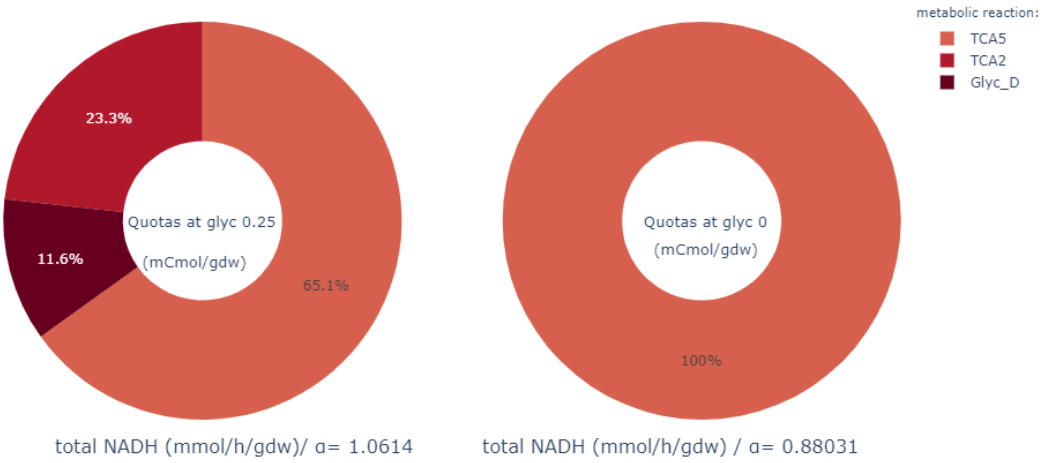

Figure 9 – Specific metabolic fluxes for NADH production in the anaerobic phase. These fluxes were obtained through the performance of two simulations for an EBPR system. The first simulation (left plot) used the quotas for the maximal foldchange at glycogen 0.25 mCmol/g_{dw}, whilst the second simulation (right plot) used the quotas for the maximal foldchange at glycogen 0 mCmol/g_{dw}. The metabolic reactions used are represented in weight percentage and the total NADH flux amount divided by the foldchange is plotted underneath. Glyc_D: glycogen degradation; TCA2: conversion isocitrate to Succinyl-CoA in the TCA cycle; TCA5: conversion of malate to oxaloacetate in the TCA cycle.

Figure 9 corroborates with the hypothesis of an overestimation of the TCA cycle. At the maximal foldchange quotas for an initial quota of 0 mCmol/$g_{dw,}$ the reducing power is being generated fully from the TCA5 reaction. The TCA5 reaction represents the malate dehydrogenase reaction, the conversion of malate to oxaloacetate. To avoid this overestimation a new simulation was created where the TCA5 reaction was blocked anaerobically (chapter 3.1.3). A thermodynamic analysis of this reaction and its consequent blockage can be found in the discussion (chapter 4.2).

In addition, the specific metabolic fluxes for NADH consumption for both a simulation of the maximal foldchange quotas at glycogen 0.25 mCmol/g_{dw} (Figure 7B – orange marker) and a simulation of maximal foldchange quotas at glycogen 0 mCmol/g_{dw} (Figure 7A – red marker) were also plotted (figure 10). In figure 10, it is possible to see that at glycogen 0 mCmol/g_{dw} the NADH generated solely from the TCA5 reaction is being equally divided into the PHB and PH_2MV synthesis reactions. In turn, at glycogen 0.25 mCmol/g_{dw}, the NADH generated is not being equally divided. In fact, the NADH generated from the glycogen degradation is fully going into PHB synthesis. Resulting in

a higher NADH consumption flux for PHB synthesis at a glycogen quota of 0.25 mCmol/g_{dw}.

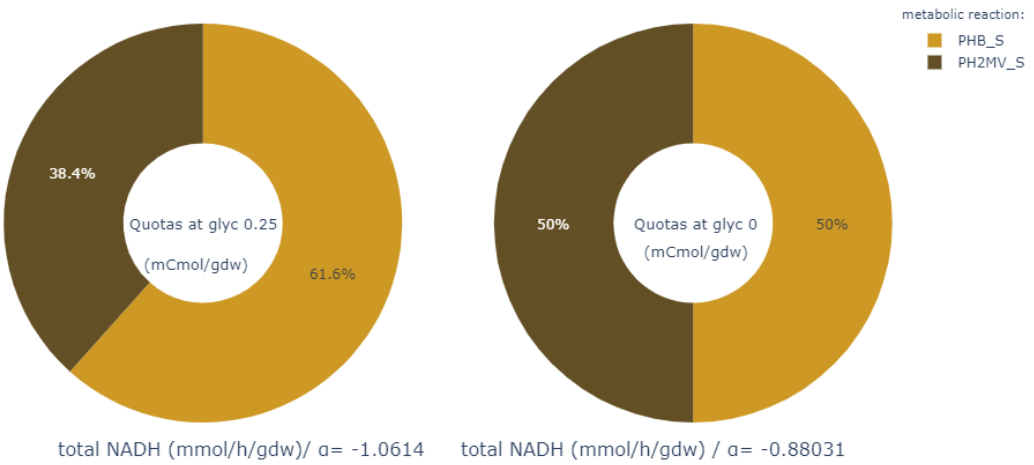

Figure 10 – Specific metabolic fluxes for NADH consumption in the anaerobic phase. These fluxes were obtained through the performance of two simulations for an EBPR system. The first simulation (left plot) used the quotas for the maximal foldchange at glycogen 0.25 mCmol/gdw, whilst the second simulation (right plot) used the quotas for the maximal foldchange at glycogen 0 mCmol/gdw. The metabolic reactions used are represented in weight percentage and the total NADH flux amount divided by the foldchange is plotted underneath. PHB_S: PHB synthesis; PH2MV_S: PH2MV synthesis.

Finally, it is important to denote that at the maximal foldchange quotas for higher glycogen amounts [0.5 - 1 mCmol/g_{dw}] it is observed the same proportion in NADH fluxes, as observed for maximal foldchange quotas at glycogen 0.25 mCmol/g_{dw}. The specific metabolic fluxes for NADH production and consumption for the maximal foldchange quotas at 0.75 mCmol/g_{dw} can be found in the supplementary information (figure S2).

3.1.3 – SIMULATION WITH THE ANAEROBIC BLOCKAGE OF THE MALATE DEHYDROGENASE REACTION

To understand the relationship between the use of glycogen and polyphosphate and how it relates to growth in a model with the TCA5 reaction blocked anaerobically, multiple simulations were performed in a similar way to the previous model. In these simulations, polyphosphate and glycogen initial quotas were set to different amounts, whilst PHA and acetate initial quotas were set to the same amounts throughout all simulations (polyphosphate vs. glycogen quotas – table 3). Each simulation was performed to a typical EBPR cycle with the metabolic model described in chapter 2.2, where the cycle ran for 5 h in time discretization of 1 hour, the first 2h represent the anaerobic phase, and the last 3 h the aerobic phase. The generated foldchange (α) in each simulation was compared in figure 11. In addition, a comparison of the modeled results with the obtained experimental work can be found in the supplementary information (figure S3),

this comparison resulted in equivalent results to the ones obtained with the previous model (figure 6).

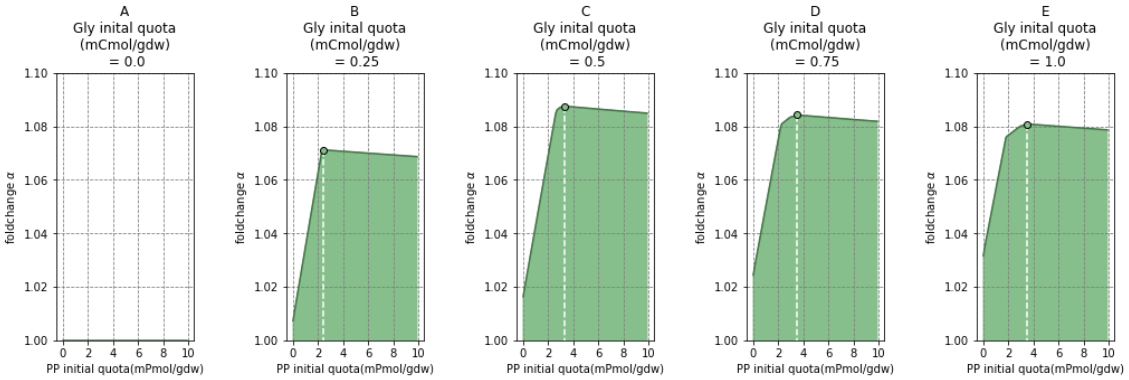

Figure 11 – Variation of foldchange (α) vs. a range of fixed initial polyphosphate (PP) and glycogen (Gly) quotas. Achieved through the performance of multiple simulations for an EBPR system where the first 2h represent the anaerobic time and the last 3h the aerobic time. Each simulation was performed with different polyphosphate (PP) initial quotas [from 0 to 10 mPmol/g_{dw}] at different fixed glycogen (Glyc) initial [0,0.25,0.5,1 mCmol/g_{dw} in steps of 0.1] resulting in a specific foldchange. Other fixed quotas used in these simulations can be found in table 3. In this simulation, reaction TCA5 was blocked anaerobically. In each graph, the highest foldchange achieved is highlighted by a marker.

The results indicate a similar relationship to the one observed in figure 7 between glycogen and polyphosphate, where the foldchange increases with the increase of polyphosphate initial quota for each simulation (figure 11B, 11C, 11D, and 11E) until it reaches an upper limit. However, with the anaerobic blockage of TCA5, the second stage of increase is smaller. The switch to the use of the glyoxylate shunt still occurs for simulations 11C,11D, and 11E. In this case, because the TCA5 reaction is blocked the system uses the reverse reaction of TCA4 (conversion of malate to succinate) to avoid malate accumulation. Similar to the previous simulation, with the increase of the initial polyphosphate amount more ATP is being generated. Hence, to produce a corresponding NADH amount to this high amount of ATP, the system switches from using the reducing branch of the TCA cycle to using the glyoxylate shunt. The system switches from consuming NADH in both the reverse reactions of TCA5 and TCA4 to just consuming NADH in the TCA4 reaction.

In simulations 11B and 11C the upper limit increases with the increase of the glycogen initial quota, while in simulations 11D and 11E the upper limit decreases. Making the maximal foldchange achieved within this simulation at a glycogen initial quota of 0.5 mCmol/g_{dw}. This suggests that in this simulation optimally there is a need for glycogen, but a higher quota than the optimal will lead to a decrease in growth. This ultimately shows a complex balance between the glycogen and polyphosphate polymers available and the environment.

It's important to note, that in simulation 11B the simulated acetate feed amount (3.84 mCmol/g_{dw}) is not being fully consumed by the simulated organism, due to having a small

initial glycogen quota amount. The remaining acetate amount is being consumed through the established competition reaction. Comparatively to the model without the TCA5 reaction blockage, this newly developed model has a higher necessity for glycogen, the highest foldchange achieved is at a glycogen quota of 0.5 mCmol/g_{dw} and not at a glycogen quota of 0.25 mCmol/g_{dw}. The system compensates for the lack of NADH being generated from the TCA5 reaction with a higher glycogen degradation, needing in turn a higher optimal glycogen amount. The respective NADH production and consumption fluxes for the maximal foldchange quotas at glycogen 0.25 and 0.5 mCmol/g_{dw} can be found in the supplementary information (figure S6).

In addition, at a glycogen initial quota of 0 mCmol/$g_{dw.}$ (figure 11A) organisms do not grow under the given simulated conditions. This behavior is following what was previously discussed, where growth with full depletion of glycogen has never been observed for PAO-type metabolism.

To investigate further this relationship a bigger range of initial quotas for glycogen (from 0 to 6 mCmol/g_{dw}) and polyphosphate (from 0 to 25 mCmol/g_{dw}) was simulated.

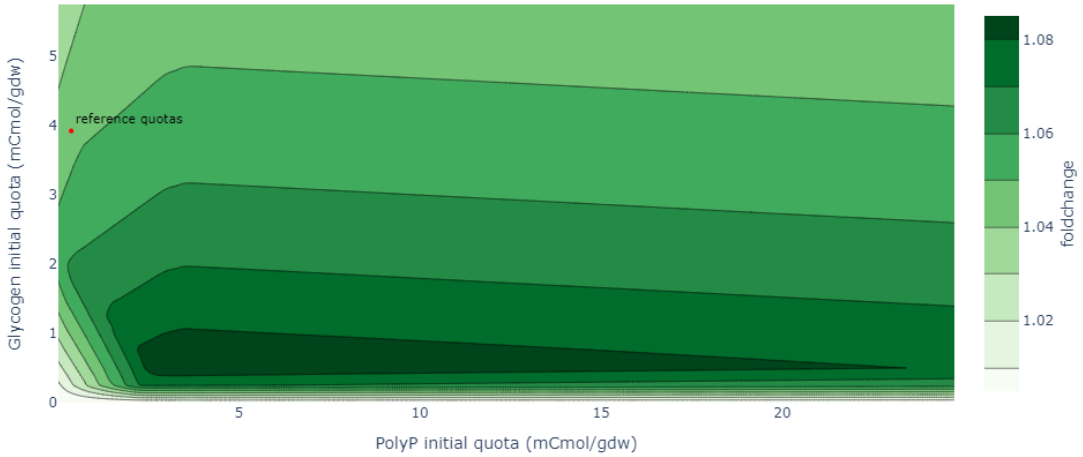

Figure 12 – Contour plot. The color gradient represents the variation of foldchange (α), in the x-axis a range of fixed initial polyphosphate (PP) is represented while in the y-axis a glycogen (Gly) initial quotas range is represented. This was achieved through the performance of multiple simulations in an EBPR system where the first 2h represent the anaerobic time and the last 3h the aerobic time. Each simulation was performed with different polyphosphate (PP) initial quotas [from 0 to 25 mPmol/g_{dw} in steps of 0.25] at different fixed glycogen (Glyc) initial [from 0 to 6 mCmol/g_{dw} in steps of 0.25] resulting in a specific foldchange. Other fixed quotas used in these simulations can be found in table 3. In this simulation, TCA5 was blocked anaerobically. The red marker indicates the reference quotas present in table 3.

This figure demonstrates an overall view of the relationship of polyphosphate and glycogen initial quotas, at specific acetate and PHA fixed quotas. Here it is possible to see an “optimal nucleus”, a range of polyphosphate initial quotas [2.1-23.5 mPmol/g_{dw} at the highest and lowest level] and glycogen quotas [0.3-1 mCmol/g_{dw} at the highest and lowest level], where the foldchange is maximal. The quotas obtained experimentally (figure 11 -red marker) are not within this nucleus, suggesting that in reality, the organism

does not grow optimally. In actuality, values within the calculated optimal range for polyphosphate have been previously reported in literature. Both (Acevedo et al., 2012) and (Laurens Welles et al., 2017) reported values within this range. However, to the extent of our knowledge glycogen values within the indicated optimal range have not been reported. In fact, Zhou and colleagues observed a minimal limit for glycogen around 1 mCmol/g_{dw} (Zhou et al., 2009). Possibly making the “optimal nucleus” unachievable in reality.

It is important to note that the PHA polymers are set to certain quotas in figure 12 (found in table 3). In supplementary information, it is possible to find simulations with different orders of magnitude for PHA polymer´s initial quotas (figure S8 and S9). In addition, the dynamic between acetate availability and the polymers glycogen (figure S5) and polyphosphate (figure S4) were also compared, and the respective graphs can be found in experimental information.

4

DISCUSSION

4.1 – CONDITIONAL FLUX BALANCE (CFBA) ASSUMPTIONS AND LIMITATIONS

Conditional flux balance analysis (cFBA) was developed in a way to create a constraint-base optimization that allows temporal metabolic changes throughout a cycle (Rugen et al., 2015). This was specially developed for organisms that grow in periodic environments, which need a modeling approach that incorporates a temporal organization into a metabolic description. In this work, this approach was applied to a PAO meta-network in a way to describe its metabolism throughout an EBPR cycle. This approach led to PAO/GAO behavior as a function of time in a specific environment defined by quotas.

This model is defined under the assumption of cyclic growth. Dynamic conditions were considered a stable cycle, where changes are consistent and predictable. Hence, in a cFBA model, the final amounts are a multiple (α) of the initial amounts (eq. 1). This assumption allows for a simulation of a time-variant metabolism. However, it does not fully allow for the temporal simulation of unstable conditions and enforces the synthesis of a certain amount of metabolites that the system might not need. This behavior can be observed in figure 11 where above the optimal proportion between glycogen and polyphosphate there is a slight decline in growth, due to resources being overspent in the synthesis of polyphosphate. In reality, while the organism might have higher amounts than the optimal to guarantee robustness, at a certain point the organism will no longer synthesize polymers to the detriment of its growth so it can meet a consistent cyclic behavior (eq.1).

Additionally, this approach has a quota feature where imbalanced metabolites can be constrained over the cycle. In this work, initial quotas were introduced to both stored polymers and acetate. These quotas set the initial metabolite amount for each simulation, making the system highly dependent on these amounts. Experimentally, polyphosphate amounts are indirectly calculated through the bulk liquid concentration of orthophosphate (eq. 42). Although the P release concentrations are consistent through experimental work, the absolute polyphosphate amount is dependent on the equation used to calculate it. In literature, there are different ways in how polyphosphate can be calculated from these concentrations, (Acevedo et al., 2012), and (Laurens Welles et al., 2017) have proposed different equations. Hence, the polyphosphate amounts indicated in this work represent an estimate that can vary with the polyphosphate equation used, making, in turn, the initial quota used for polyphosphate and the simulations performed dependent on this equation (eq. 42).

Finally, most cFBA models developed use an enzymatic constrain, where each flux is constrained by the amount of the respective enzyme and each enzyme amount is

constrained by the amount of ribosomes. In this work, this feature was not used, and a general enzyme and ribosome synthesis reaction was created and fixed throughout all time points. In this thesis, multiple simulations are performed, which demand high computational power, introducing additional enzyme capacities constraints for all reactions would hinder the multiple simulations created. Additionally, looking at figure 8 is possible to see that the model created generates comparable results to reality without enzymatic constrain. As a matter of fact, da Silva and colleagues investigated the effect of different enzyme capacities in a cFBA PAO meta-network through sensitivity analysis (da Silva et al., 2019). This sensitivity analysis indicated that most simulations were not sensitive to changes in k_{cat} across 3 orders of magnitude. However, the obtained trade-offs in this thesis may be dependent on the unlimited fluxes used. Hence, further constraining reaction fluxes with enzyme capacities might change the resulting phenotype of the system (Wissel, 2021).

4.2 –METABOLIC NETWORK ASSUMPTIONS AND LIMITATIONS

The metabolic network created in this thesis was based on the meta-network developed in (da Silva et al., 2019). The key difference between the published model (figure S9) and the model developed in this work (figure 5) is the expansion of the TCA cycle reactions. In actuality, (da Silva et al., 2019) model had three representative reactions for the TCA cycle, red TCA indicating the reductive branch of the TCA cycle, ox TCA indicating the oxidative branch of the TCA cycle, and Gox TCA indicating the glyoxylate shunt. These reactions were expanded in this thesis creating seven distinctive TCA reactions (TCA1-7). In this work, we want to explore the energy trade-off, and the TCA cycle together with glycogen represent the sources for reducing power in PAO metabolism. Hence, by expanding the TCA cycle is possible to pinpoint the working TCA reactions that generate reducing power in a PAO simulation. This is observed in figure 9 where it was possible to pinpoint that the TCA5 reaction was being overestimated in this model.

In addition, throughout this work, two TCA reactions were blocked anaerobically: TCA4 and TCA5. TCA4 represents the conversion of succinate to malate (succinate dehydrogenase) and TCA5 represents the conversion of malate to oxaloacetate (malate dehydrogenase). TCA4 was assumed to be only active aerobically due to the succinate dehydrogenase reaction producing $FADH_2$. Regeneration to the FAD form is deemed to be unlikely to happen in the absence of an electron acceptor (O_2), so this reaction was blocked anaerobically in all simulations (Mino et al., 1998).

TCA5 was blocked due to an overestimation of the reducing power being generated from the TCA cycle within the present model (figure 9). Based on the literature, (Wexler et al., 2009) observed, through radiolabelling proteomics, that the malate dehydrogenase enzyme (MDH) was more prevalent aerobically. This might suggest that the TCA5 reaction is not fully active or blocked in the anaerobic phase corroborating with the assumption made in this model.

To further investigate the feasibility of this reaction, a thermodynamic analysis was performed on TCA5. A reaction is thermodynamic feasible when it is in compliance with the second law of thermodynamics $\Delta_r G < 0$. The Gibbs free energy of a reaction ($\Delta_r G$) can be estimated through equation 43 (assuming the reaction $A + B \leftrightarrow C + D$).

$$\Delta_r \boldsymbol{G} = \left[\Delta_f \boldsymbol{G_C} + \Delta_f \boldsymbol{G_D} - \Delta_f \boldsymbol{G_A} - \Delta_f \boldsymbol{G_B}\right] + \boldsymbol{RTln}\left(\frac{[\boldsymbol{C}] \cdot [\boldsymbol{D}]}{[\boldsymbol{A}] \cdot [\boldsymbol{B}]}\right) \quad \textbf{(43)}$$

Where $\Delta_f G_x$ denotes the standard Gibbs formation energy for each species, R is the universal gas constant, T is the absolute temperature (298.15 K) and $[X]$ represents the species concentration.

This equation (eq.43) was adapted to the malate dehydrogenase reaction (eq.34):

$$\Delta_r \boldsymbol{G} = \boldsymbol{26.5 \pm 0.06} + \boldsymbol{RTln}\left(\frac{[\boldsymbol{OAA}] \cdot [\boldsymbol{NADH}]}{[\boldsymbol{MAL}] \cdot [\boldsymbol{NAD}]}\right) \quad \textbf{(44)}$$

Equation 44 denotes that the sum of the Gibbs formation energy for all species is positive, making the thermodynamic viability of the reaction highly dependent on metabolite concentration. In turn, the NADH/NAD ratio is affected by the presence of oxygen (Sun et al., 2012). Hence, the resulting $\Delta_r G$ of TCA5 is dependent on the presence of oxygen. To study this dependence, the $\Delta_r G$ was plotted against different ratios of NADH/NAD (figure 13).

In this plot, the Δ_fG of each species and the Keq were retrieved from (*Equilibrator*, n.d.), the $[MAL]$ concentration was retrieved from (*Bioblast*, n.d.),the $[OAA]$ concentration was estimated from the Keq, and the aerobic/anaerobic literature NADH/NAD ranges were retrieved from (Bekers et al., 2015).

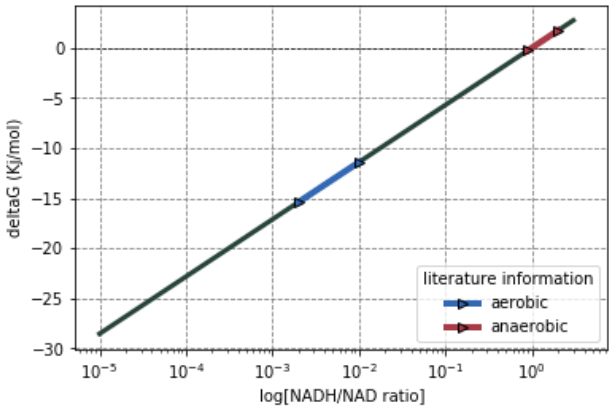

Figure 13 – Variation of $\Delta_r G$ of the malate dehydrogenase reaction with different NADH/NAD ratios. The $\Delta_r G$ was calculated through equation 44. Additionally, the figure indicates the experimentally observed range for NADH/NAD for aerobic (blue) and anaerobic (red) conditions.

Figure 13 indicates that for the observed NADH/NAD ranges in anaerobic conditions the $\Delta_r G$ can be positive, demonstrating that in anaerobic conditions the TCA5 reaction is not thermodynamically viable. In contrast, for observed aerobic ranges the $\Delta_r G$ is negative demonstrating that in aerobic conditions the TCA5 reaction is thermodynamically viable. These observations are further validated by (Kiparissides & Hatzimanikatis, 2017) work, where a Thermodynamics-based metabolic sensitive analysis (TMSA) was performed to a TCA cycle metabolic network. They observed that the MDH reaction exhibited a thermodynamic shift in response to metabolite concentrations and that in anaerobic conditions, perturbations in the metabolite concentrations altered the directionality of the reaction.

4.3 – LITERATURE COMPARISON OF THE OBSERVED TRADE-OFF BETWEEN THE USE OF GLYCOGEN AND POLYPHOSPHATE

As indicated in figure 2, Welles and colleagues investigated the trade-off between glycogen and polyphosphate in a PAO culture by adjusting this culture to increase phosphate concentrations in the feed (Laurens Welles et al., 2017). This led to an increase in stored polyphosphate amount and a corresponding decline in stored glycogen amount (figure 2). These results demonstrate a decreasing tendency of a PAOs enrichment to move towards the “optimal nucleus” observed in figure 12. However, the last data point does not meet this decreasing profile, possibly indicating a start of a stabilizing behavior. As it was mentioned before, Zhou and colleagues reported a glycogen minimal limit around 1 mCmol/g_{dw} making the “optimal nucleus” out of range (Zhou et al., 2009).

This minimal limit could be a consequence of how glycogen is determined experimentally. Glycogen is quantified as glucose after acid digestion. Therefore, non-glycogen glucose-containing biomass components are being quantified as glycogen through this method. Hence, the minimal limit observed could be a background glucose amount, and glycogen, in reality, is being fully consumed. However, Damir and colleagues calculated this non-glycogen glucose overestimation and reported a result of 0.22 ± 0.03 mCmol/g_{dw}(Damir Brdjanovic et al., 1998), thus this does not fully explain the minimal glycogen limit. This minimal glycogen amount could also be a safety precaution. In truth, having quotas within the “optimal nucleus” might present a risky behavior. Being within this nucleus might lead to optimal growth, however minimal changes in these quotas could lead to no growth at all. To easily observe this risk, the foldchange for a range of initial glycogen quotas [0-6 mCmol/g_{dw}] at a fixed polyphosphate initial quota of 6 mPmol/g_{dw} was plotted (figure 14). In figure 14, the section highlighted in green represents the glycogen range in the “optimal nucleus observed in figure 11”. Here, it's possible to see that a minimal decrease in glycogen can lead to a fall in growth.

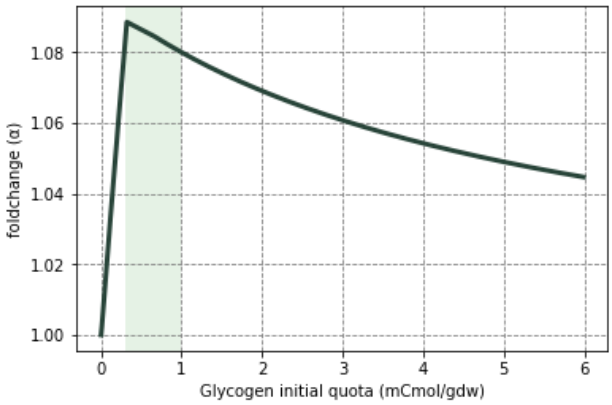

Figure 14 – Foldchange variation in multiple simulations in an EBPR system where the first 2h represent the anaerobic time and the last 3h the aerobic time. Each simulation was performed with a fixed polyphosphate (PP) initial quota of 6 mPmol/g_{dw} at different fixed glycogen (Glyc) initial [from 0 to 6 mCmol/g_{dw}] resulting in a specific foldchange. Other fixed quotas used in these simulations can be found in table 3.

This “safety precaution” could show a robustness behavior on the organism’s part. As it was mentioned before, robustness can be defined as the resilience in face of uncertainty. It represents the expected loss of opportunity, which in this case is the opportunity for growth. If the organisms had glycogen amounts within the optimal range a minimal change in the environment could lead to no growth, thus the organism would not possess the resilience to uncertain changes in the environment. Hence, although having higher amounts of glycogen will lead to a smaller growth (loss of efficiency) it will also lead to a gain of robustness making the organism more fit to uncertain changes in the environment.

5

CONCLUSION AND FUTURE WORK

5.1- CONCLUSION

Below is possible to see a list of the primary conclusions of this work.

- There is a clear trade-off between the use of glycogen and polyphosphate in an EBPR cycle. Phosphate accumulating organisms have the metabolic flexibility to trade-off between the synthesis of each polymer according to the resources available in the environment and thus affecting the growth of the organism.

- Optimal growth for PAOs in an EBPR environment was observed within a range of polyphosphate [2.1-23.5 mPmol/g_{dw}] and glycogen [0.3-1 mCmol/g_{dw}] initial amounts.

- To the extent of our knowledge, growth with the optimal range of glycogen amounts observed and growth with full depletion of glycogen has never been reported in PAOs literature. This suggests a glycogen minimal limitation for PAOs in an EBPR cycle.

- This glycogen minimal limit (e.g. 1 mCmol/g_{dw}) suggests a robustness mechanism employed by PAOs.

- A thermodynamic analysis was performed on the malate dehydrogenase reaction (TCA5), which led to the conclusion that TCA5 is not feasible in an anaerobic environment.

5.2- FUTURE WORK

- A thermodynamic analysis should be done to all the present reactions in the metabolic network and the model should be further constricted. Creating a combination between a cFBA model and TFBA (thermodynamic-based flux balance analysis) model.

- The glycogen minimal limit should be further validated and investigated through experimental work.

- To simulate unstable environments more closely related to reality, a new dynamic FBA model should be established that forgoes the assumption of cyclic growth.

Symbol/ Abbreviation	*Description*
P	Phosphorus
EBPR	Enhanced biological phosphate removal
PAOs	Phosphate accumulating organisms
VFA	Volatile fatty acid
Ac	Acetate
Pr	Propionate
PHA	poly-ß-hydroxyalkanoates
PolyP / PP	Polyphosphate
Glyc	Glycogen
PAM	Phosphate accumulating metabolism
PHB	Poly-β-hydroxybutyrate
PHV	poly-β-hydroxyvalerate
PH2MV	poly-β-hydroxy-2-methylvalerate
GAOs	Glycogen accumulating organisms
GAM	Glycogen accumulating metabolism
FBA	Flux balance analysis
LP	Linear programming
S	Stoichiometric matrix
cFBA approach	
cFBA	Conditional flux balance analysis
Sb	Stoichiometric matrix for balanced metabolites
Si	Stoichiometric matrix for imbalanced metabolites
v^k	Flux distribution in the k^{th} time-interval
M(t)	Imbalanced metabolite amounts at the t time-step
α	Foldchange, the definition of growth in a cFBA approach
w^t	Weight matrix
C^kquota	Quota value for the k^{th} time-point
B^kquota	Index matrix for the corresponding *C^kquota*
b_{low}	Lower bound
b_{up}	Upper bound
Metabolic network	
Ac_upt	Uptake of external acetate.
Glyc S	Glycogen synthesis.
Glyc D	Glycogen degradation.
PEPC	Phosphoenolpyruvate formation.

PEPCK	Phosphoenolpyruvate carboxykinase.
BMP S	Biomass precursors synthesis
Enzymes S	General enzyme synthesis.
Ribosomes S	General ribosome synthesis.
PHB S	PHB synthesis.
PHB D	PHB degradation.
PH2MV S	PH2MV synthesis.
PH2MV D	PH2MV degradation.
PP S	Polyphosphate Synthesis.
PP D	Polyphosphate degradation.
ETC	Electron transport chain
CO2 exp	CO_2 export.
Vcomp	Competition acetate uptake
Ac feed	Fake replenishment of acetate reaction.
TCA1	Conversion of Oxaloacetate to Isocitrate in the TCA cycle.
TCA2	Conversion of Isocitrate to Succinyl- CoA in the TCA cycle.
TCA3	Conversion of Succinyl-CoA to succinate in the TCA cycle.
TCA4	Conversion of Succinate to Malate in the TCA cycle.
TCA5	Conversion of Malate to oxaloacetate in the TCA cycle.
TCA6	Conversion of isocitrate to succinate in the glyoxylate shunt.
TCA7	Conversion of Acetyl-CoA to malate in the glyoxylate shunt.
PR	Conversion of pyruvate to malate in pyruvate metabolism.
PDH1	Pyruvate dehydrogenase.
PDHD	Pyruvate dehydrogenase.
Experimental work	
SBR	Sequencing batch reactor
TSS	Total suspended solids
VSS	Volatile suspended solids
GC	Gas chromatography
ΔG_f	Gibbs free energy of formation
ΔG_r	Gibbs free energy of the reaction
K_{eq}	Equilibrium constant
K_{cat}	Enzyme turnover number.

6

REFERENCES

Acevedo, B., Oehmen, A., Carvalho, G., Seco, A., Borrás, L., & Barat, R. (2012). Metabolic shift of polyphosphate-accumulating organisms with different levels of polyphosphate storage. *Water Research*, *46*(6), 1889–1900. https://doi.org/10.1016/j.watres.2012.01.003

Bekers, K. M., Heijnen, J. J., & van Gulik, W. M. (2015). Determination of the in vivo NAD: NADH ratio in Saccharomyces cerevisiae under anaerobic conditions, using alcohol dehydrogenase as sensor reaction. *Yeast*, *32*(8), 541–557. https://doi.org/10.1002/YEA.3078

Bioblast. (n.d.). Retrieved October 13, 2021, from https://www.bioblast.at/index.php/Malate

Bordel, S. (2011). A metabolic network of a phosphate-accumulating organism provides new insights into enhanced biological phosphorous removal. *Water Science and Technology*, *64*(12), 2410–2416. https://doi.org/10.2166/wst.2011.787

Brdjanovic, D., Van Loosdrecht, M. C. M., Hooijmans, C. M., Mino, T., Alaerts, G. J., & Heijnen, J. J. (1998). Effect of polyphospbate limitation on the anaerobic metabolism of phosphorus-accumulating microorganisms. *Applied Microbiology and Biotechnology*, *50*(2), 273–276. https://doi.org/10.1007/s002530051289

Brdjanovic, Damir, van Loosdrecht, M. C. M., Hooijmans, C. M., Mino, T., Alaerts, G. J., & Heijnen, J. J. (1998). Bioassay for glycogen determination in biological phosphorus removal systems. *Water Science and Technology*, *37*(4–5), 541–547. https://doi.org/10.2166/WST.1998.0715

da Silva, L. G., Gamez, K. O., Gomes, J. C., Akkermans, K., Welles, L., Abbas, B., Loosdrecht, M. C. M. va., & Wahl, S. A. (2020). Revealing the Metabolic Flexibility of “Candidatus Accumulibacter phosphatis” through Redox Cofactor Analysis and Metabolic Network Modeling. *Applied and Environmental Microbiology*, *86*(24), 1–17. https://doi.org/10.1128/AEM.0808-20

da Silva, L. G., Tomás-Martínez, S., van Loosdrecht, M. C. M., & Wahl, S. A. (2019). The environment selects: Modeling energy allocation in microbial communities under dynamic environments. *BioRxiv*. https://doi.org/10.1101/689174

equilibrator. (n.d.). Retrieved October 13, 2021, from https://equilibrator.weizmann.ac.il/search?query=malate+%2B+nad+%3D+nadh+%2B+oxaloacetate&x=0&y=0

Gianchandani, E. P., Chavali, A. K., & Papin, J. A. (2010). The application of flux balance analysis in systems biology. *Wiley Interdisciplinary Reviews: Systems Biology and Medicine*, *2*(3), 372–382. https://doi.org/10.1002/wsbm.60

KEGG GENOME T00966. (n.d.). Retrieved August 29, 2021, from https://www.genome.jp/dbget-bin/get_linkdb?-t+pathway+gn:T00966

Kiparissides, A., & Hatzimanikatis, V. (2017). Thermodynamics-based Metabolite

Sensitivity Analysis in metabolic networks. *Metabolic Engineering*, *39*(November 2016), 117–127. https://doi.org/10.1016/j.ymben.2016.11.006

Louie, T. M., Mah, T. J., Oldham, W., & Ramey, W. D. (2000). Use of metabolic inhibitors and gas chromatography/mass spectrometry to study poly-β-hydroxyalkanoates metabolism involving cryptic nutrients in enhanced biological phosphorus removal systems. *Water Research*, *34*(5), 1507–1514. https://doi.org/10.1016/S0043-1354(99)00302-4

Majed, N., Chernenko, T., Diem, M., & Gu, A. Z. (2012). Identification of functionally relevant populations in enhanced biological phosphorus removal processes based on intracellular polymers profiles and insights into the metabolic diversity and heterogeneity. *Environmental Science and Technology*, *46*(9), 5010–5017. https://doi.org/10.1021/es300044h

Martín, H. G., Ivanova, N., Kunin, V., Warnecke, F., Barry, K. W., McHardy, A. C., Yeates, C., He, S., Salamov, A. A., Szeto, E., Dalin, E., Putnam, N. H., Shapiro, H. J., Pangilinan, J. L., Rigoutsos, I., Kyrpides, N. C., Blackall, L. L., McMahon, K. D., & Hugenholtz, P. (2006). Metagenomic analysis of two enhanced biological phosphorus removal (EBPR) sludge communities. *Nature Biotechnology*, *24*(10), 1263–1269. https://doi.org/10.1038/nbt1247

McPhail, C., Maier, H. R., Kwakkel, J. H., Giuliani, M., Castelletti, A., & Westra, S. (2018). Robustness Metrics: How Are They Calculated, When Should They Be Used and Why Do They Give Different Results? *Earth's Future*, *6*(2), 169–191. https://doi.org/10.1002/2017EF000649

Mino, T., Van Loosdrecht, M. C. M., & Heijnen, J. J. (1998). Microbiology and biochemistry of the enhanced biological phosphate removal process. *Water Research*, *32*(11), 3193–3207. https://doi.org/10.1016/S0043-1354(98)00129-8

Oehmen, A., Lemos, P. C., Carvalho, G., Yuan, Z., Keller, J., Blackall, L. L., & Reis, M. A. M. (2007). Advances in enhanced biological phosphorus removal: From micro to macro scale. *Water Research*, *41*(11), 2271–2300. https://doi.org/10.1016/j.watres.2007.02.030

Oyserman, B. O., Noguera, D. R., Del Rio, T. G., Tringe, S. G., & McMahon, K. D. (2016). Metatranscriptomic insights on gene expression and regulatory controls in Candidatus Accumulibacter phosphatis. *ISME Journal*, *10*(4), 810–822. https://doi.org/10.1038/ismej.2015.155

Pardelha, F., Albuquerque, M. G. E., Reis, M. A. M., Dias, J. M. L., & Oliveira, R. (2012). Flux balance analysis of mixed microbial cultures: Application to the production of polyhydroxyalkanoates from complex mixtures of volatile fatty acids. *Journal of Biotechnology*, *162*(2–3), 336–345. https://doi.org/10.1016/j.jbiotec.2012.08.017

Pereira, H., Lemos, P. C., Reis, M. A. M., Crespo, J. P. S. G., Carrondo, M. J. T., & Santos, H. (1996). Model for carbon metabolism in biological phosphorus removal processes based on in vivo13C-NMR labelling experiments. *Water Research*, *30*(9), 2128–2138. https://doi.org/10.1016/0043-1354(96)00035-8

Perez-Garcia, O., Lear, G., & Singhal, N. (2016). Metabolic network modeling of microbial interactions in natural and engineered environmental systems. *Frontiers in Microbiology*, *7*(MAY). https://doi.org/10.3389/fmicb.2016.00673

Pirt, S. J. (1987). The energetics of microbes at slow growth rates: Maintenance energies and dormant organisms. *Journal of Fermentation Technology*, *65*(2), 173–177. https://doi.org/10.1016/0385-6380(87)90161-0

Rugen, M., Bockmayr, A., & Steuer, R. (2015). Elucidating temporal resource allocation and diurnal dynamics in phototrophic metabolism using conditional FBA. *Scientific Reports*, *5*(September), 1–16. https://doi.org/10.1038/srep15247

Schuler, A. J., & Jenkins, D. (2003). Enhanced Biological Phosphorus Removal from Wastewater by Biomass with Different Phosphorus Contents, Part I: Experimental Results and Comparison with Metabolic Models. *Water Environment Research*, *75*(6), 485–498. https://doi.org/10.2175/106143003x141286

Smolders, G. J. F., van der Meij, J., van Loosdrecht, M. C. M., & Heijnen, J. J. (1994). Model of the anaerobic metabolism of the biological phosphorus removal process: Stoichiometry and pH influence. *Biotechnology and Bioengineering*, *43*(6), 461–470. https://doi.org/10.1002/bit.260430605

Sun, F., Dai, C., Xie, J., & Hu, X. (2012). Biochemical Issues in Estimation of Cytosolic Free NAD/NADH Ratio. *PLOS ONE*, *7*(5), e34525. https://doi.org/10.1371/JOURNAL.PONE.0034525

van Loosdrecht, M. C. M., Nielsen, P. H., Lopez-Vazquez, C. M., & Brdjanovic, D. (2016). Experimental Methods in Wastewater Treatment. In *Water Intelligence Online* (Vol. 15). https://doi.org/10.2166/9781780404752

Vargas, M., Yuan, Z., & Pijuan, M. (2013). Effect of long-term starvation conditions on polyphosphate- and glycogen-accumulating organisms. *Bioresource Technology*, *127*, 126–131. https://doi.org/10.1016/j.biortech.2012.09.117

Welles, L., Lopez-Vazquez, C. M., Hooijmans, C. M., van Loosdrecht, M. C. M., & Brdjanovic, D. (2016). Prevalence of 'Candidatus Accumulibacter phosphatis' type II under phosphate limiting conditions. *AMB Express*, *6*(1). https://doi.org/10.1186/s13568-016-0214-z

Welles, Laurens, Abbas, B., Sorokin, D. Y., Lopez-Vazquez, C. M., Hooijmans, C. M., van Loosdrecht, M. C. M., & Brdjanovic, D. (2017). Metabolic response of "candidatus accumulibacter phosphatis" clade II C to changes in influent P/C ratio. *Frontiers in Microbiology*, *7*(JAN). https://doi.org/10.3389/fmicb.2016.02121

Wexler, M., Richardson, D. J., & Bond, P. L. (2009). Radiolabelled proteomics to determine differential functioning of Accumulibacter during the anaerobic and aerobic phases of a bioreactor operating for enhanced biological phosphorus removal. *Environmental Microbiology*, *11*(12), 3029–3044. https://doi.org/10.1111/j.1462-2920.2009.02007.x

Wissel, D. (2021). *Developing a metabolic analysis tool using observed enzyme amounts for dynamic conditions*.

Yagci, N., Artan, N., Çokgör, E. U., Randall, C. W., & Orhon, D. (2003). Metabolic model for acetate uptake by a mixed culture of phosphate- and glycogen-accumulating organisms under anaerobic conditions. *Biotechnology and Bioengineering*, *84*(3), 359–373. https://doi.org/10.1002/bit.10765

Zhou, Y., Pijuan, M., Zeng, R. J., Lu, H., & Yuan, Z. (2008). Could polyphosphate-accumulating organisms (PAOs) be glycogen-accumulating organisms (GAOs)? *Water Research*, *42*(10–11), 2361–2368. https://doi.org/10.1016/j.watres.2008.01.003

Zhou, Y., Pijuan, M., Zeng, R. J., & Yuan, Z. (2009). Involvement of the TCA cycle in the anaerobic metabolism of polyphosphate accumulating organisms (PAOs). *Water Research*, *43*(5), 1330–1340. https://doi.org/10.1016/j.watres.2008.12.008

7.1 – EXPERIMENTAL INFORMATION

7.1.1 – DETERMINATION OF THE MAINTENANCE FLUX

To validate the developed model and calculate initial quotas for the respective simulations, an experimental EBPR system was created (figure 8). This experiment had a constant sludge retention time of 8 days, in which the external orthophosphate concentration and the internal PHA and glycogen amounts were being monitored.

The maintenance coefficient was determined through the external orthophosphate profile (figure S1). In the anaerobic period, orthophosphate increases in the liquid bulk (polyphosphate is being consumed), this increase has two distinct phases (A and B). Where A represents the polyphosphate consumption that generates ATP for both maintenance and acetate uptake. Whilst B represents polyphosphate consumption that generates ATP for maintenance. Hence, the maintenance flux can calculate through the slope of the B phase (0.0241 mPmol/g_{dw}.h), resulting in a maintenance coefficient of 0.03 mmol ATP/g_{dw}.h. It's important to note that maintenance requirements shift with the changes in aeration (Pirt, 1987), however in this work they are assumed to be the same.

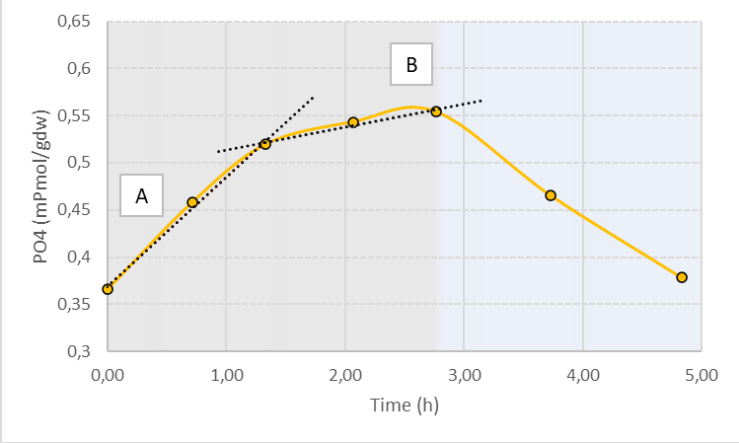

Figure S1 – orthophosphate (PO4) profile through time in a PAO enrichment in an EBPR system. The reactor operation and polymer determination information can be found in chapter x. A) trendline for the first 3 time points in the anaerobic phase ($y = 0.1158x + 0.3688$; $R^2 = 0.99$). B) trendline for the last 3 time points in the anaerobic phase ($y = 0{,}0241x + 0{,}4895$; $R^2 = 0{,}96$).

The calculated experimental amounts determined through the methods described in chapter 2.3, can be found in the following table S1. Highlighted in grey are the amounts obtained in the anaerobic phase, and in blue are the amounts obtained in the aerobic phase.

Table S1 – Metabolite amounts through time in a 6h SBR cycle for a PAO enrichment (chapter 2.3.1). The determination methods for these amounts can be found in chapter 2.3.

PHA (mCmol/gdw)	**Glycogen** (mCmol/gdw)	**Poly-P** (mCmol/gdw)	**PO_4** (mCmol/gdw)	**Acetate** (mCmol/gdw)
1.68	3.92	0.38	0.37	3.84
3.36	3.24	0.29	0.46	
5.36	2.61	0.22	0.52	
6.00	2.22	0.20	0.54	
5.13	2.23	0.19	0.55	0.34
2.56	4.17	0.28	0.47	
1.03	5.41	0.37	0.38	

Additionally, a carbon balance was performed to the determined amounts (table S2). As we know, it's important to note that CO_2 release was not measured.

Table S2 – Carbon balance to the obtained experimental amounts (table S1). The amounts were obtained through time in a 6h SBR cycle for a PAO enrichment (chapter 2.3).

Anaerobic (mCmol/gdw)		**Aerobic (mCmol/gdw)**	
PHA produced	4.32	PHA consumed	-4.10
Glycogen consumed	-1.69	Glycogen produced	3.17
Acetate consumed	-3.5		
C balance	-0.87	C balance	-0.92

7.2 – ADITIONAL INFORMATION FOR SIMULATION WITHOUT TCA5 BLOCKAGE

7.2.1 - NADH CONSUMPTION

The specific metabolic fluxes for NADH consumption for both a simulation with the maximal foldchange quotas at glycogen 0.25 mCmol/g_{dw} (Figure 7B – orange marker) and with the maximal foldchange quotas at glycogen 0 mCmol/g_{dw} (Figure 7A – red marker) were plotted (figure S2).

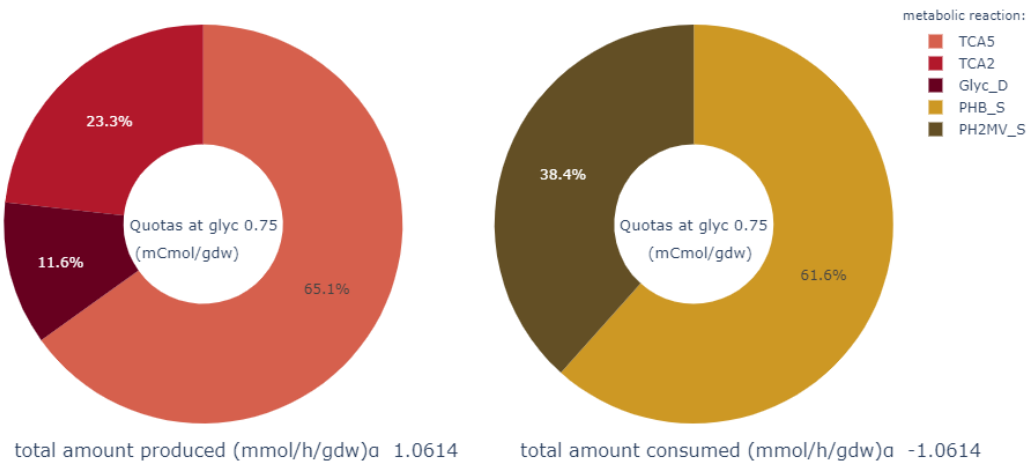

Figure S2 – Specific metabolic fluxes for NADH production (left) and consumption (right) in the anaerobic phase. These fluxes were obtained through the performance of two simulations in an EBPR system. Both simulations used the maximal foldchange quotas at glycogen 0.75 mCmol/gdw. The metabolic reactions used are represented in weight percentage and the total NADH flux amount divided by the foldchange is plotted underneath the pie plots.

7. 3 - ADDITIONAL INFORMATION FOR SIMULATION WITH TCA5 BLOCKAGE

7.3.1 – EXPERIMENTAL COMPARISON

A simulation with the TCA5 reaction blocked anaerobically was generated in a typical EBPR cycle with the metabolic model described in chapter 2.2. The cycle ran for 5 h in time discretization of 1 hour, where the first 2h represent the anaerobic phase and the last 3 h the aerobic phase. An LP optimization was performed where each polymer was constrained to specific initial amounts based on experimental data (table 3 -reference quotas).

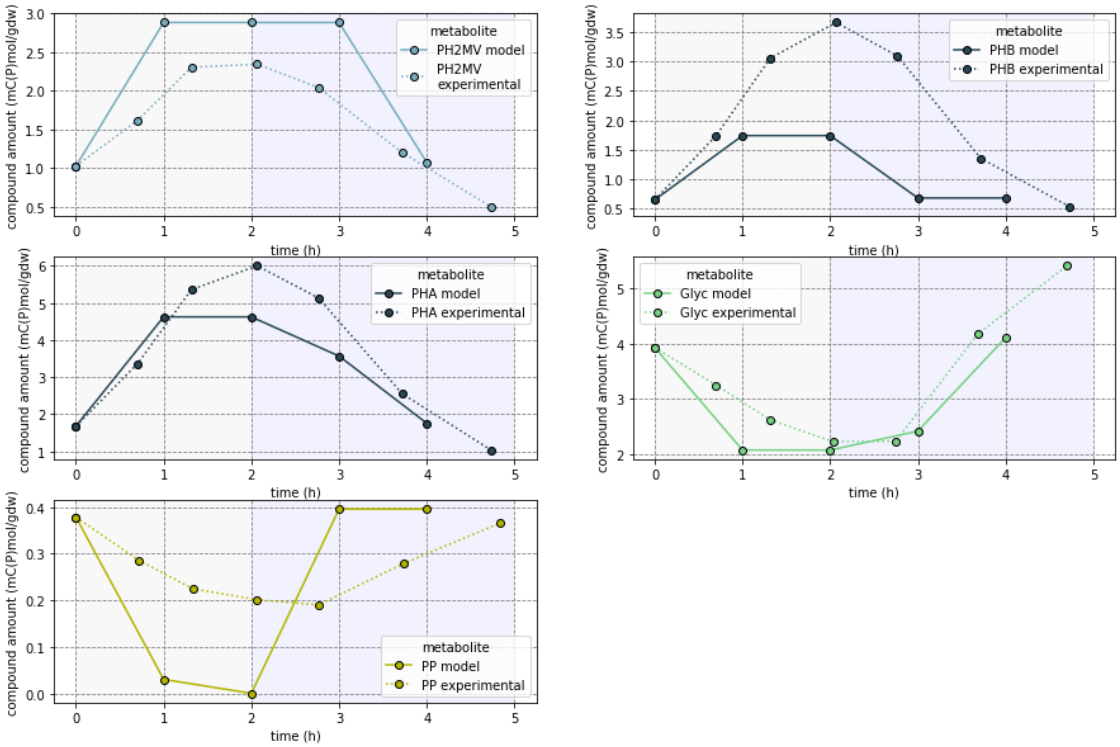

Figure S3 - Metabolic concentrations of polymers through time in a cFBA simulation (model – full lines) and SBR operation (experimental – dotted lines) in an EBPR system. The first 2h represent the anaerobic time and the last 3h the aerobic time. For the model results, the initial quotas used can be found in table 3 (reference quotas) and the complete reactions and model restrictions can be found in chapter 2.2, the resulting foldchange was 1.046. For the experimental results, the reactor operation and polymer determination information can be found in chapter 2.3.

In the following figure S3, the behavior between the polyphosphate amount initially stored and Acetate availability is studied.

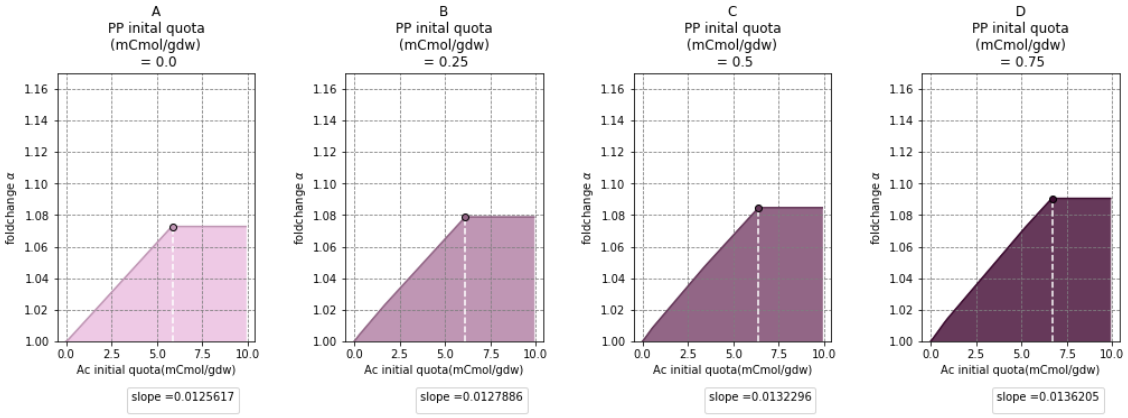

Figure S4 – Variation of foldchange (α) vs. a range of fixed initial polyphosphate (PP) and acetate (Ac) quotas. Achieved through the performance of multiple PAO simulations in an EBPR system where the first 2h represent the anaerobic time and the last 3h the aerobic time. Each simulation was performed with different Acetate (Ac) initial quotas [from 0 to 10 mCmol/g_{dw}] at different fixed polyphosphate (PP) initial quotas [0,0.25,0.5,0.75 mPmol/g_{dw}]. resulting in a specific foldchange. Other fixed quotas used in these simulations can be found in table 3. In this simulation, TCA5 was blocked anaerobically. In each simulation, the maximal foldchange is highlighted with a marker.

The results indicate a relationship between polyphosphate and acetate for organisms living under the conditions tested (figure S3). The foldchange increases with the increase of Acetate initial quota for each simulation (A, B, C, D, E) until it reaches an upper limit and stabilizes. This upper limit represents the optimal proportion between Acetate and polyphosphate. At higher amounts of acetate, the organism doesn't have the resources to fully uptake the acetate available, so acetate is further consumed by competition (table 1 – vcomp). The observed upper limit increases with the increase of the polyphosphate initial quota, demonstrating that the highest foldchange achieved in this simulation was at a polyphosphate quota of 0.75 mCmol/g_{dw}. Finally, simulation A demonstrates growth with the absence of polyphosphate indicating a GAO-type behavior.

In the following figure S4, the behavior between the glycogen amount initially stored and Acetate availability is studied.

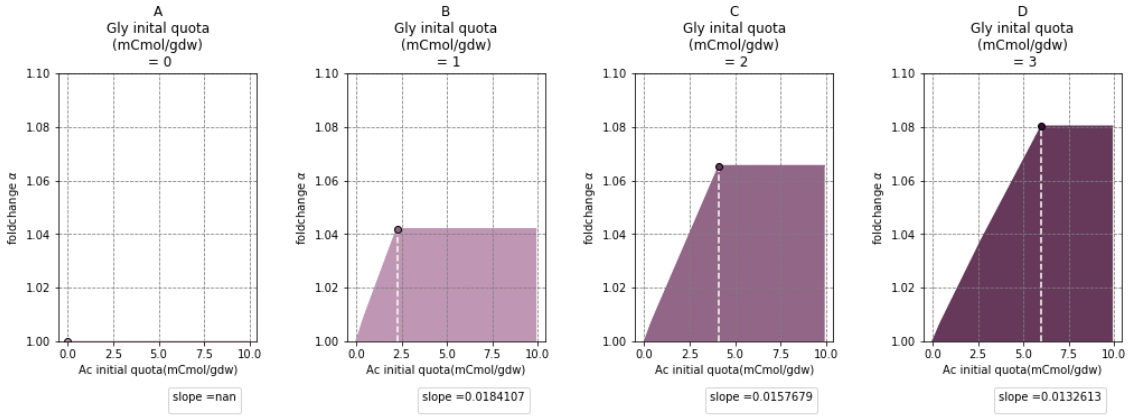

Figure S5 – Variation of foldchange (α) vs. a range of fixed initial glycogen (Glyc) and acetate (Ac) quotas. Achieved through the performance of multiple PAO simulations in an EBPR system where the first 2h represent the anaerobic time and the last 3h the aerobic time. Each simulation was performed with different Acetate (Ac) initial quotas [from 0 to 10 mCmol/g_{dw}] at different fixed glycogen (Glyc) initial quotas [0,1,2,3 mPmol/g_{dw}]. resulting in a specific foldchange. Other fixed quotas used in these simulations can be found in table 3. In this simulation, TCA5 was blocked anaerobically. In each simulation, the maximal foldchange is highlighted with a marker.

The results indicate a relationship between glycogen and acetate for organisms living under the conditions tested (figure S4). There is no growth observed in absence of glycogen (simulation A). The foldchange increases with the increase of Acetate initial quota for each simulation (B, C, D, E) until it reaches an upper limit and stabilizes. This upper limit represents the optimal proportion between Acetate and glycogen. At higher amounts of acetate, the organism doesn't have the resources to fully uptake the acetate available, so acetate is further consumed by competition (table 1 – vcomp). The observed upper limit increases with the increase of the polyphosphate initial quota, demonstrating that the highest foldchange achieved in this simulation was at a glycogen quota of 0.75 mCmol/g_{dw}. However, it is important to note that the slope decreases with each simulation. Hence, at lower amounts of acetate, a higher foldchange will be achieved at lower fixed glycogen quotas, whilst at higher acetate amounts higher foldchange will be achieved at higher fixed glycogen quotas.

The specific metabolic fluxes for NADH production (left) and consumption(right) for a simulation with the fixed quotas were plotted (figure S5).

Figure S6 – Specific metabolic fluxes for NADH production (left) and consumption (right) in the anaerobic phase. These fluxes were obtained through the performance of four simulations in an EBPR system. A) Simulations that used the maximal foldchange quotas at glycogen 0.25 mCmol/gdw. B) A) Simulations that used the maximal foldchange quotas at glycogen 0.5 mCmol/gdw. The metabolic reactions used are represented in weight percentage and the total NADH flux amount is plotted underneath the pie plots. In this simulation, TCA5 was blocked anaerobically.

10 times higher

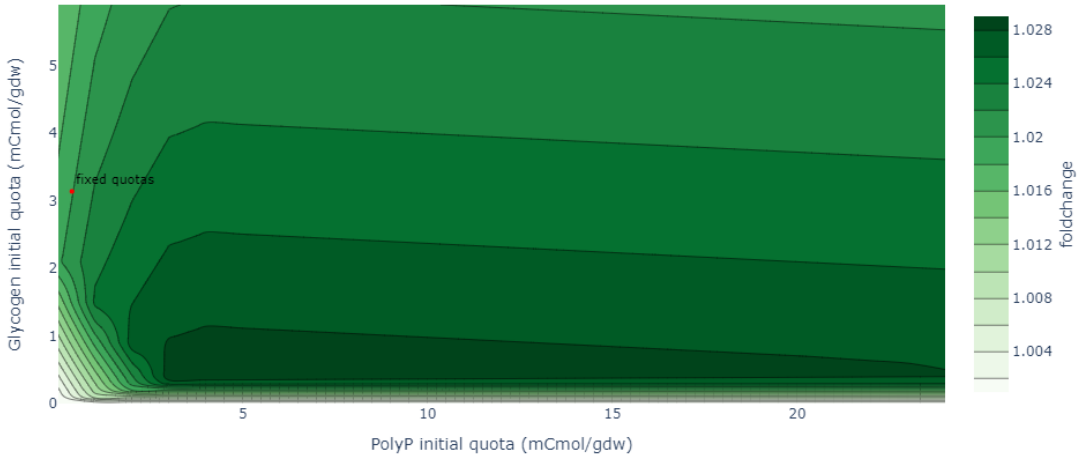

Figure S7 – Contour plot where the color gradient represents the variation of foldchange (α), in the x-axis a range of fixed initial polyphosphate (PP) is represented while in the y-axis a glycogen (Gly) initial quotas range is represented. This was achieved through the performance of multiple PAO simulations in an EBPR system where the first 2h represent the anaerobic time and the last 3h the aerobic time. Each simulation was performed with different polyphosphate (PP) initial quotas [from 0 to 10 mPmol/g_{dw}] at different fixed glycogen (Glyc) initial [from 0 to 5 mCmol/g_{dw}] resulting in a specific foldchange. Other fixed quotas used in these simulations can be found in table 3, PHA quotas were fixed 10 times higher than the amount indicated in Table 3. In this simulation, TCA5 was blocked anaerobically.

10 times lower

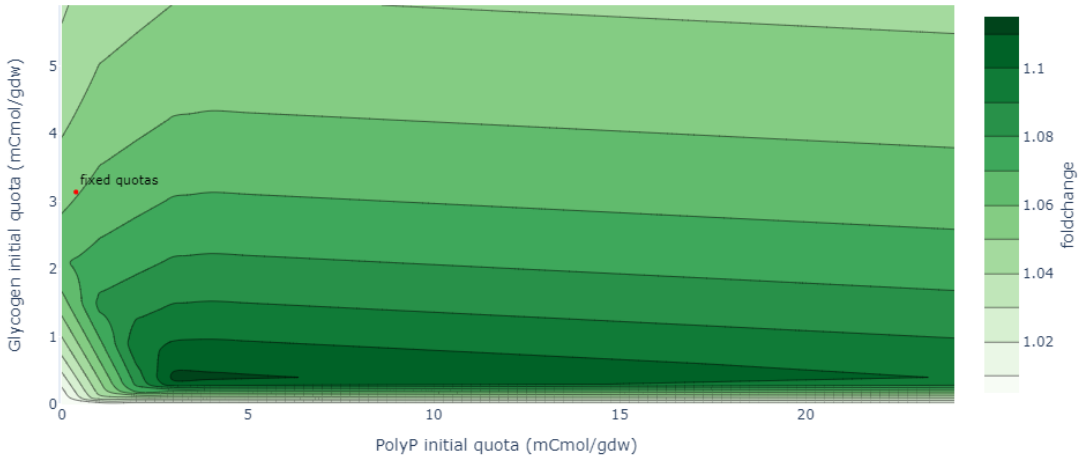

Figure S8 – Contour plot where the color gradient represents the variation of foldchange (α), in the x-axis a range of fixed initial polyphosphate (PP) is represented while in the y-axis a glycogen (Gly) initial quotas range is represented. This was achieved through the performance of multiple PAO simulations in an EBPR system where the first 2h represent the anaerobic time and the last 3h the aerobic time. Each simulation was performed with different polyphosphate (PP) initial

quotas [from 0 to 10 mPmol/g_{dw}] at different fixed glycogen (Glyc) initial [from 0 to 5 mCmol/g_{dw}] resulting in a specific foldchange. Other fixed quotas used in these simulations can be found in table 3, PHA quotas were fixed 10 times lower than the amount indicated in Table 3. In this simulation, TCA5 was blocked anaerobically.

Figures S6 and S7 indicate that higher fixed PHA quotas will lead to a lower achieved foldchange (α) and vice-versa. Resources that were previously being used towards growth are now being used towards PHA synthesis, resulting in a decrease in growth.

7.4 – ADDITIONAL INFORMATION FOR THE METABOLIC NETWORK AND ITS IMPLEMENTATION

7.4.1 – ORIGINAL METABOLIC MODEL

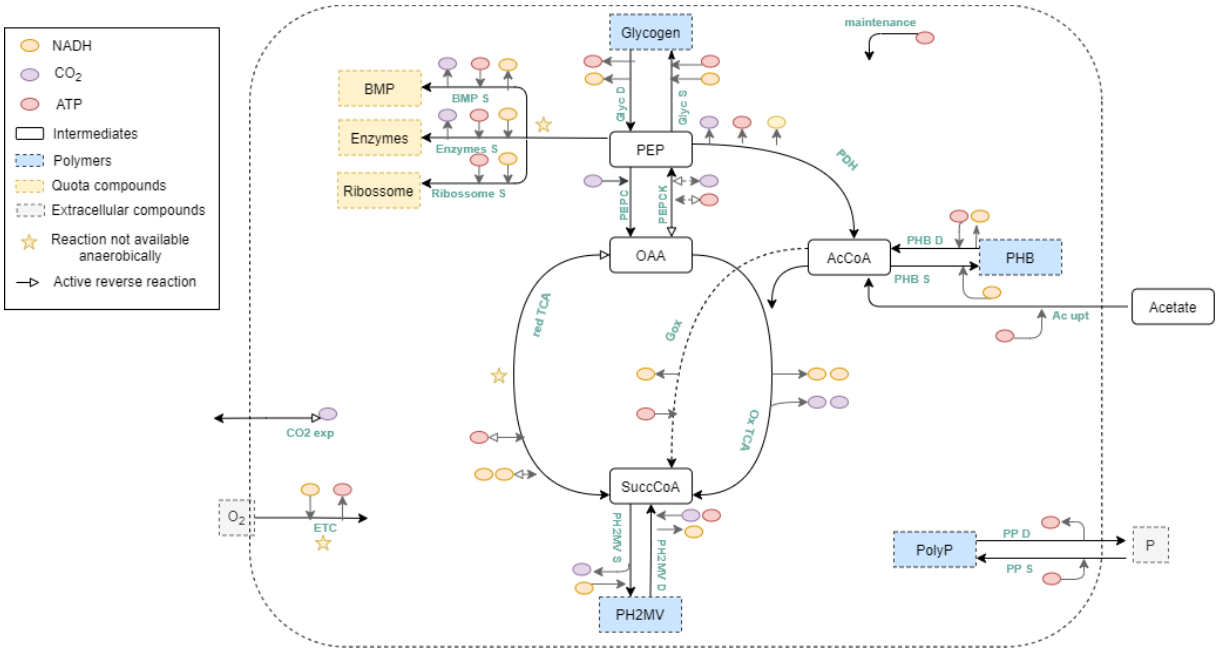

Figure S9 – Representation of the (da Silva et al., 2019) model. Meta-network for Phosphate accumulating organism. Glyc D, S: glycogen degradation and synthesis reactions; BMP S: Biomass precursors synthesis reaction; Enzymes S: general enzymatic synthesis reaction; Ribosome S: general ribosome synthesis reaction; PDH: pyruvate dehydrogenase reaction; PEPC: Phosphoenolpyruvate formation reaction; PEPCK: Phosphoenolpyruvate carboxykinase reaction; PHB D, S: PHB degradation and synthesis reaction; Ac up: Acetate uptake reaction; GOX: glyoxylate shunt; Ox TCA: oxidative branch of the TCA cycle; red TCA: reductive branch of the TCA cycle; PH2MV D, S: PH2MV degradation and synthesis reaction; ETC: electron transport chain; CO_2 exp: CO_2 export reaction; PP D, S: polyphosphate degradation and synthesis.

Stochiometric matrix (S_mat)

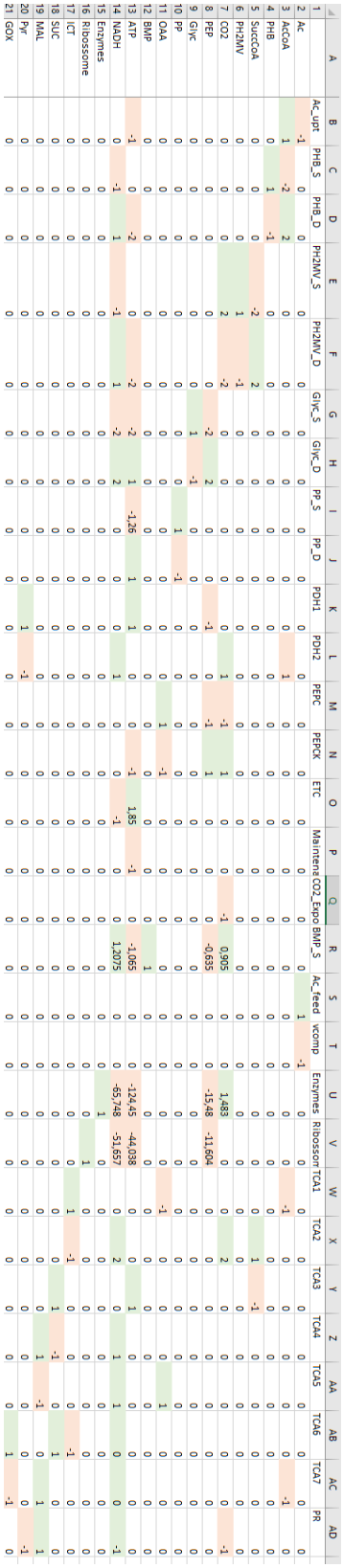

	A	B	C	D	E	F	G	H	I	J	K	L	M	N	O	P	Q	R	S	T	U	V	W	X	Y	Z	AA	AB	AC	AD
1		Ac_upt	PHB_S	PHB_D	PH2MV_S	PH2MV_D	Glyc_S	Glyc_D	PP_S	PP_D	PDH1	PDH2	PEPC	PEPCK	ETC	Maintena	CO2_Expo	BMP_S	Ac_feed	vcomp	Enzymes	Ribosson	TCA1	TCA2	TCA3	TCA4	TCA5	TCA6	TCA7	PR
2	Ac	-1	0	0	0	0	0	0	0	0	0	0	0	0	0	0	0	0	1	-1	0	0	0	0	0	0	0	0	0	0
3	AcCoA	1	-2	2	0	0	0	0	0	0	0	1	0	0	0	0	0	0	0	0	0	0	-1	0	0	0	0	0	-1	0
4	PHB	0	1	-1	0	0	0	0	0	0	0	0	0	0	0	0	0	0	0	0	0	0	0	0	0	0	0	0	0	0
5	SuccCoA	0	0	0	-2	2	0	0	0	0	0	0	0	0	0	0	0	0	0	0	0	0	0	1	-1	0	0	0	0	0
6	PH2MV	0	0	0	1	-1	0	0	0	0	0	0	0	0	0	0	0	0	0	0	0	0	0	0	0	0	0	0	0	0
7	CO2	0	0	0	2	-2	0	0	0	0	0	0	0	0	0	0	-1	0	0	0	0	0	0	0	0	0	0	0	0	-1
8	PEP	0	0	0	0	0	-2	2	0	0	0	1	-1	1	0	0	0	0	0	0	1,483	0	0	0	0	0	0	0	0	0
9	Glyc	0	0	0	0	0	1	-1	0	0	0	0	0	0	0	0	0	0	0	0	-15,48	0	0	0	0	0	0	0	0	0
10	PP	0	0	0	0	0	0	0	1	-1	0	0	0	0	0	0	0	0	0	0	0	0	0	0	0	0	0	0	0	0
11	OAA	0	0	0	0	0	0	0	0	0	0	0	1	-1	0	0	0	0	0	0	0	-11,604	0	0	0	0	0	0	0	0
12	BMP	0	0	0	0	0	0	0	-1,26	1	0	0	0	0	0	0	0	1	0	0	0	0	-1	0	0	0	1	0	0	0
13	ATP	-1	0	-2	0	-2	-2	1	0	0	1	0	0	-1	1,85	-1	0	-1,065	0	0	-124,45	-44,038	0	0	1	0	0	0	0	0
14	NADH	0	-1	1	-1	1	-2	2	0	1	0	1	0	0	-1	0	0	1,2075	0	0	-65,748	-51,657	0	2	0	1	1	0	0	-1
15	Enzymes	0	0	0	0	0	0	0	0	0	0	0	0	0	0	0	0	0	0	0	1	1	0	0	0	0	0	0	0	0
16	Ribossome	0	0	0	0	0	0	0	0	0	0	0	0	0	0	0	0	0	0	0	0	1	0	0	0	0	0	0	0	0
17	ICT	0	0	0	0	0	0	0	0	0	0	0	0	0	0	0	0	0	0	0	0	0	1	0	0	0	0	0	0	0
18	SUC	0	0	0	0	0	0	0	0	0	0	0	0	0	0	0	0	0	0	0	0	0	1	-1	0	1	0	0	0	0
19	MAL	0	0	0	0	0	0	0	0	0	0	0	0	0	0	0	0	0	0	0	0	0	0	0	1	0	0	0	1	0
20	Pyr	0	0	0	0	0	0	0	0	0	0	-1	0	0	0	0	0	0	0	0	0	0	0	0	0	1	1	0	0	0
21	GOX	0	0	0	0	0	0	0	0	0	0	0	0	0	0	0	0	0	0	0	0	0	0	0	0	0	0	0	-1	0

Balanced metabolites (Balanced_mets)

	A
1	AcCoA
2	SuccCoA
3	CO2
4	PEP
5	OAA
6	ATP
7	NADH
8	ICT
9	SUC
10	MAL
11	Pyr
12	GOX

Imbalanced metabolites (Imbalanced_mets)

	A
1	Ac
2	PHB
3	PH2MV
4	Glyc
5	PP
6	BMP
7	Enzymes
8	Ribossome

Lower Bound (lb_var)

time	1	2	3	4	5
Ac_upt	0	0	0	0	0
PHB_S	0	0	0	0	0
PHB_D	0	0	0	0	0
PH2MV_S	0	0	0	0	0
PH2MV_D	0	0	0	0	0
Glyc_S	0	0	0	0	0
Glyc_D	0	0	0	0	0
PP_S	0	0	0	0	0
PP_D	0	0	0	0	0
PDH1	0	0	0	0	0
PDH2	0	0	0	0	0
PEPC	0	0	0	0	0
PEPCK	-1000	-1000	-1000	-1000	0
ETC	0	0	0	0	0
Maintenance	0,03	0,03	0,03	0,03	0
CO2_Export	-1000	-1000	-1000	-1000	0
BMP_D	0	0	0	0	0
Ac_feed	0	0	0	0	0
vcomp	0	0	0	0	0
Enzymes	0	0	0	0	0
Ribossome	0	0	0	0	0
TCA1	0	0	0	0	0
TCA2	0	0	0	0	0
TCA3	-1000	-1000	-1000	-1000	0
TCA4	-1000	-1000	-1000	-1000	0
TCA5	-1000	-1000	-1000	-1000	0
TCA6	0	0	0	0	0
TCA7	0	0	0	0	0
PR	0	0	0	0	0

Upper bound (ub_var)

time	1	2	3	4	5
Ac_upt	1000	1000	1000	1000	0
PHB_S	1000	1000	1000	1000	0
PHB_D	1000	1000	1000	1000	0
PH2MV_S	1000	1000	1000	1000	0
PH2MV_D	1000	1000	1000	1000	0
Glyc_S	1000	1000	1000	1000	0
Glyc_D	1000	1000	1000	1000	0
PP_S	1000	1000	1000	1000	0
PP_D	1000	1000	1000	1000	0
PDH1	1000	1000	1000	1000	0
PDH2	1000	1000	1000	1000	0
PEPC	1000	1000	1000	1000	0
PEPCK	1000	1000	1000	1000	0
ETC	0	0	1000	1000	0
Maintenance	0,03	0,03	0,03	0,03	0
CO2_Export	1000	1000	1000	1000	0
BMP_D	0	0	1000	1000	0
Ac_feed	0	0	0	0	1000
vcomp	1000	1000	1000	1000	0
Enzymes	0	0	1000	1000	0
Ribossome	0	0	1000	1000	0
TCA1	1000	1000	1000	1000	0
TCA2	1000	1000	1000	1000	0
TCA3	1000	1000	1000	1000	0
TCA4	0	0	1000	1000	0
TCA5	0	0	1000	1000	0
TCA6	1000	1000	1000	1000	0
TCA7	1000	1000	1000	1000	0
PR	1000	1000	1000	1000	0